Electronic Supplementary Material (ESI) for Dalton Transactions.

Modulation of phosphine sulfonate ligands containing copper complexes emission properties: playing with solvato-, thermo-, and mechanochromism

Antoine Vacher,[a] Anissa Amar,[b] Franck Camerel,[a] Yann Molard,[a] Camille Latouche,[c] Thierry Roisnel,[a] Vincent Dorcet,[a] Abdou Boucekkine,[a*] Huriye Akdas-Kiliç [a*] and Mathieu Achard [a*]

General Information:

All reactions were carried out under argon atmosphere using Schlenk tube techniques. Unless stated, reagents were purchased from commercial sources and used as received. Acetonitrile, was dried using a MBraun Solvent Purification System. Methanol HPLC grade was degassed and used as received. NMR spectra were recorded at room temperature on a Bruker Avance (400 MHz) spectrometer and reported in ppm. Data are reported as follows: s=singlet, d=doublet, t=triplet, q=quartet, m=multiplet, br=broad. Coupling constants are reported in Hz. ^{13}C NMR spectra were recorded at 100.6 MHz on the same spectrometer and reported in ppm.

Solid state absolute quantum yield were measured with a Hamamatsu C9920-03G system. Optical microscopy investigations were performed on a Nikon H600L polarising microscope equipped with a Linkam "liquid crystal pro system" hotstage. The microscope is also equipped with a UV irradiation source (Hg Lamp, λ = 340-380 nm) and an ocean optic USB 2000+ UV-Vis-NIR spectrophotometer based on CCD detection technology. This set-up allows the recording of luminescence spectra on solids, liquids, liquid crystalline materials and gels from -196°C up to 420°C between 350 and 1100 nm.

Excitation and emission spectra were recorded on a FL920 Edingburgh Instruments spectrometer, equipped with a Xenon lamp (Xe900), double monochromators for the excitation and emission pathways, and photomultiplier (PMT-R928P) as detector. The emission was collected at right angles to the excitation source with the emission wavelength selected using a double grated monochromator and detected by a R928-P PMT. The excitation and emission spectra were fully corrected using the standard corrections supplied by the manufacturer for the spectral power of the excitation source and the sensitivity of the detector.

The luminescence lifetimes were measured on a FL920 Edingburgh Instruments spectrometer, via Multichannel Scaling Module using a μF900 pulsed 60 W xenon microsecond flash lamp, with a repetition rate of 100 Hz. Low temperature measurements were performed with an Optistat cryostat with ITC controller (Liquid nitrogen).

Computational details : Computations have been performed using the B3PW91[1–3] functional together with the LANL2DZ[4–7] basis set augmented with polarization functions on all atoms except hydrogens. The choice of this pair functional-basis set is coming from our previous calculations which led to satisfying geometries and accurate optical properties simulations (absorption, emission)[8–12]. In order to accurately model our system, solvent effects (MeOH) were taken into account using implicit solvent (PCM) together with explicit molecules in the calculations.[13,14] The geometries of the ground state and of the excited states have been relaxed and frequency calculations have been performed in order to check to be at the minimum of the potential energy surfaces. UV-vis absorption and emission for the singlet states have been performed within the TD-DFT ansatz using both the B3PW91 and the CAM-B3LYP functionals.[15] The choice of the latter functional is assessed by the potential presence of a long-distance electron transfer during optical processes. Molecular orbital plots, spin orbital plots and spin density plots have been realized with the Gaussview package.[16] Oscillator strengths analysis and bands assignments were performed thanks to the VMS package.[17]

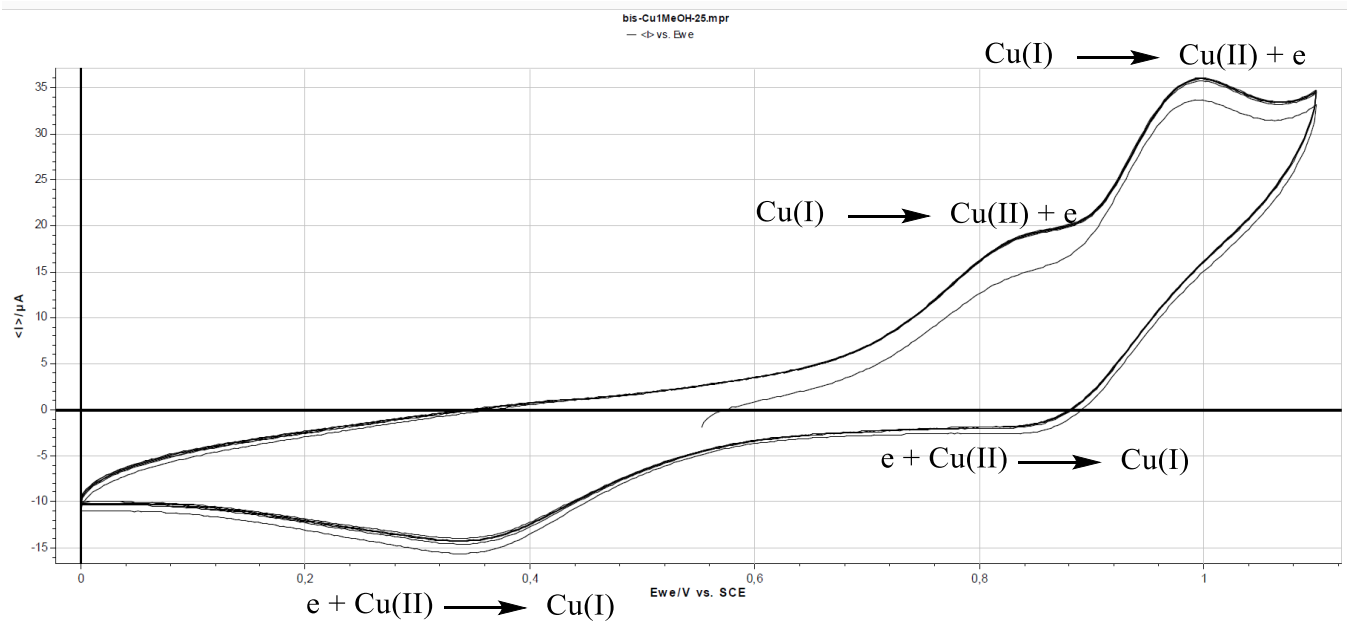

Figure S1: Cyclic voltammogram of complex **Cu-1** in methanol. The two reduction peaks suggest a dimeric structure after the first oxidation. E_{ox1} = 810 mV (irr.)/E_{Ox2}= 980 mV (quasi rev.) and E_{red1}= 860 mV (quasi rev.)/E_{red2}= 370mV (irr.)

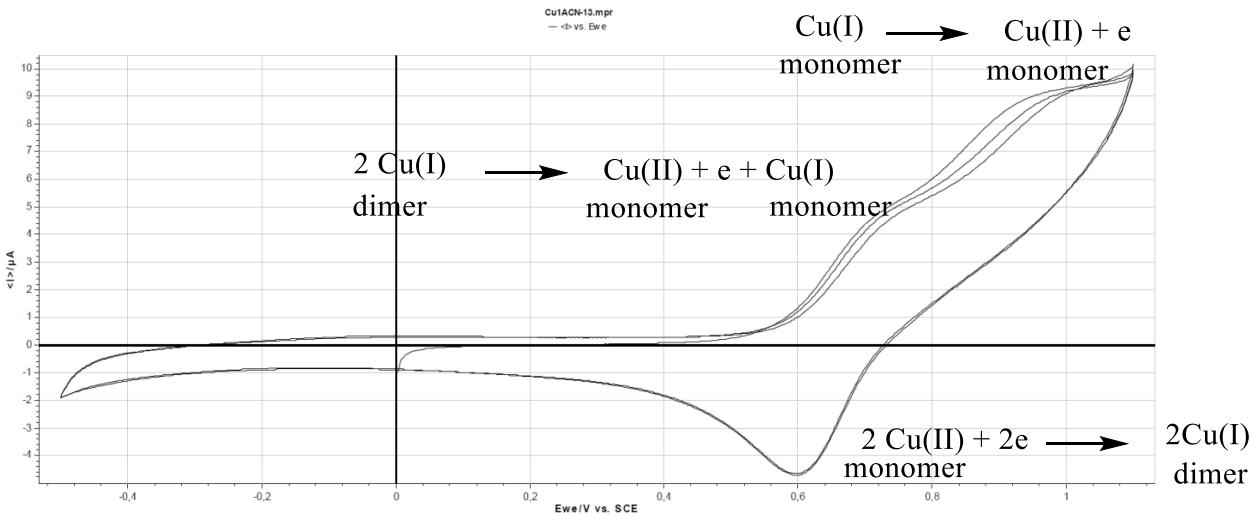

Figure S2: Cyclic voltammogram of complex **Cu-2** in acetonitrile. The presence of one reduction peak suggest a non-dimeric form after oxidation of the first copper atom. E_{ox1} = 670 mV (rev.)/E_{Ox2}= 850 mV (irr.) and E_{red1}= 600 mV (rev.).

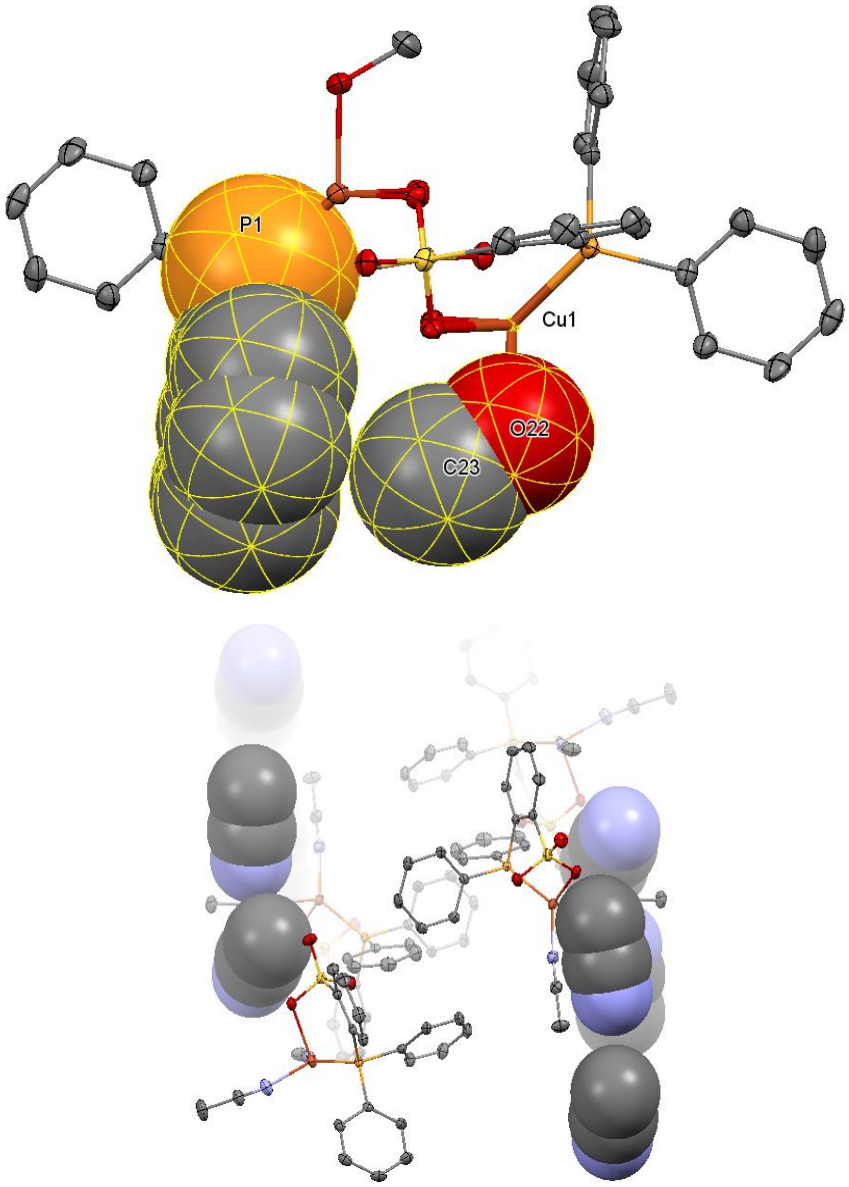

Figure S3: Effect of the solvent molecules toward rigidification via intramolecular interaction in **Cu-1** (top view) and contribution of acetonitrile in the lattice towards rigidification in **Cu-2**.

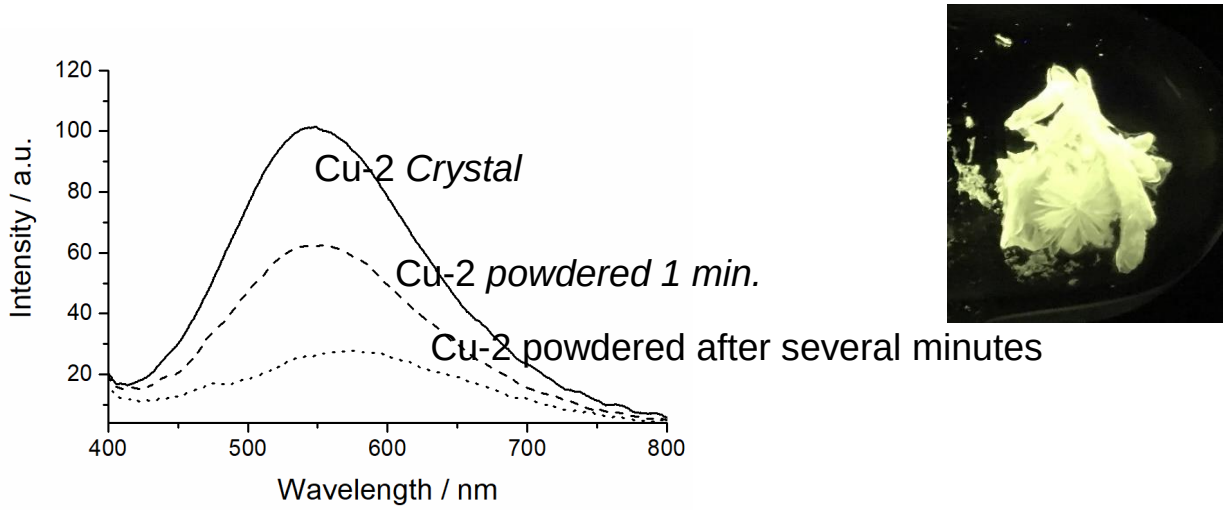

Figure S4: Evolution of the quantum yield of **Cu-2**

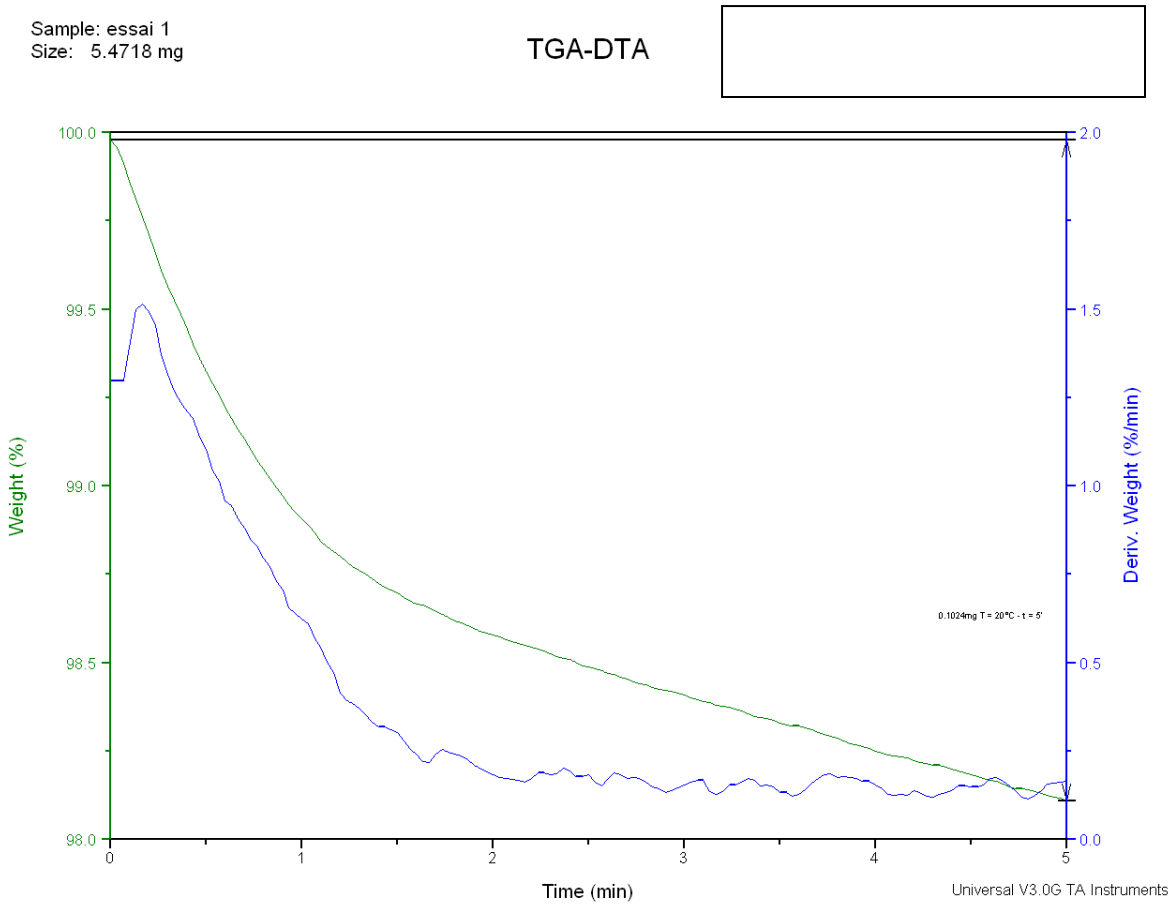

Figure S5 : TGA of (0-5 min. at 20°C) **Cu-2**

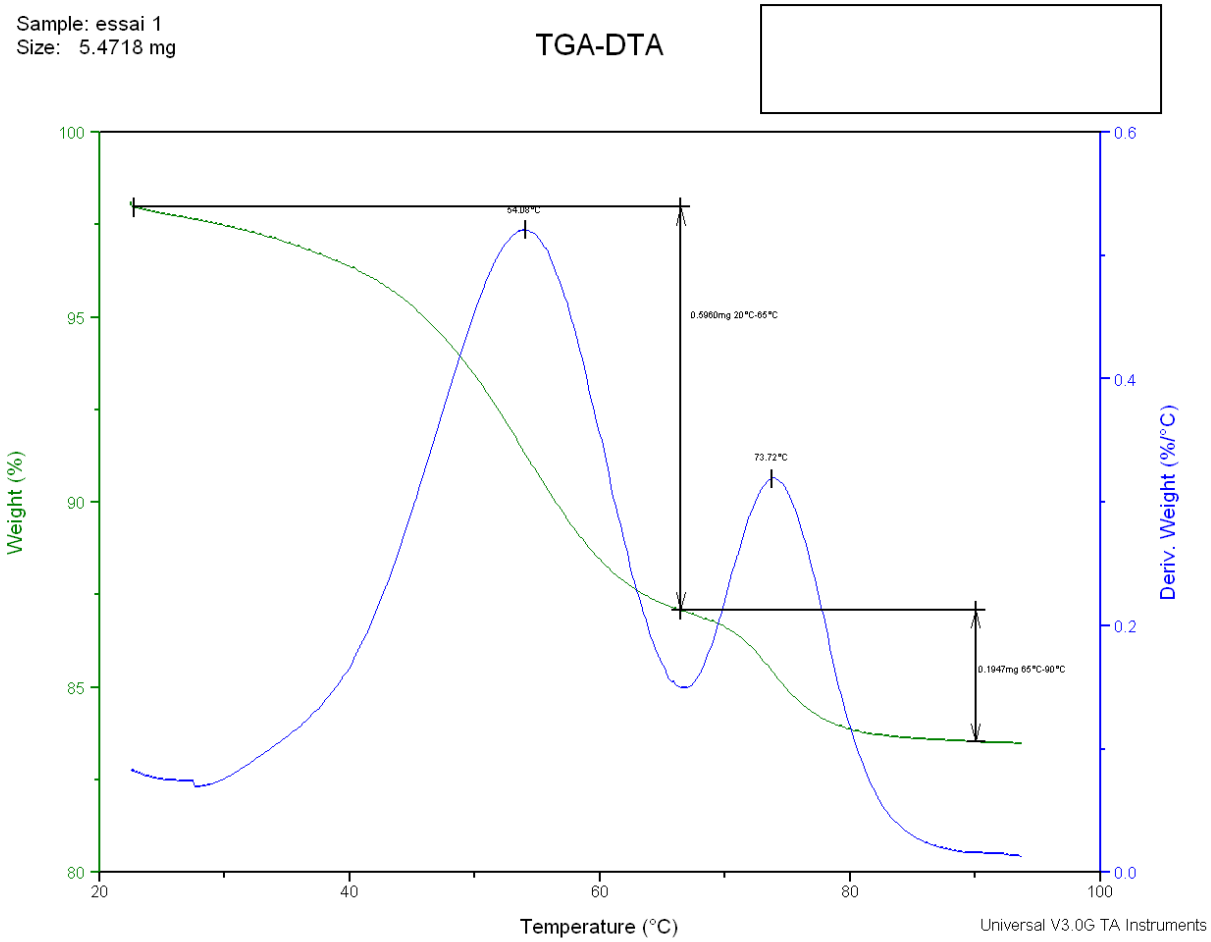

Figure S6 : TGA of **Cu-2** after 5 min. (gradient 20°C-100°C)

	QuantumYield	
1 : t= 0	0.127	--- Pristine
2	0.129	--- powdered
3	0.126	---
4 : t= 30 mins	0.168	--- addition of methanol
5	0.167	---
6 : t= 60 mins	0.167	---
7 : t= 16 h	0.033	
8	0.033	---
9	0.033	---

Figure S7 : Evolution of the quantum yield of **Cu-4**

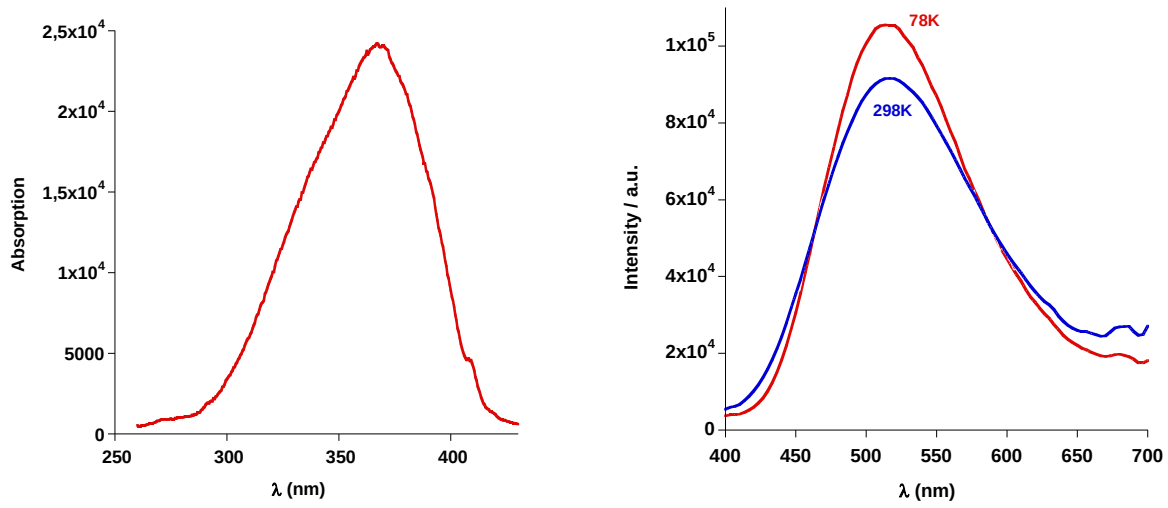

Figure S8: Excitation scan of **Cu-1** (298K, λ_{max}= 368 nm) and Emissions at 78K λ_{max}= 515 nm and 298K λ_{max}= 515 nm of **Cu-1** (Ex at 360 nm)

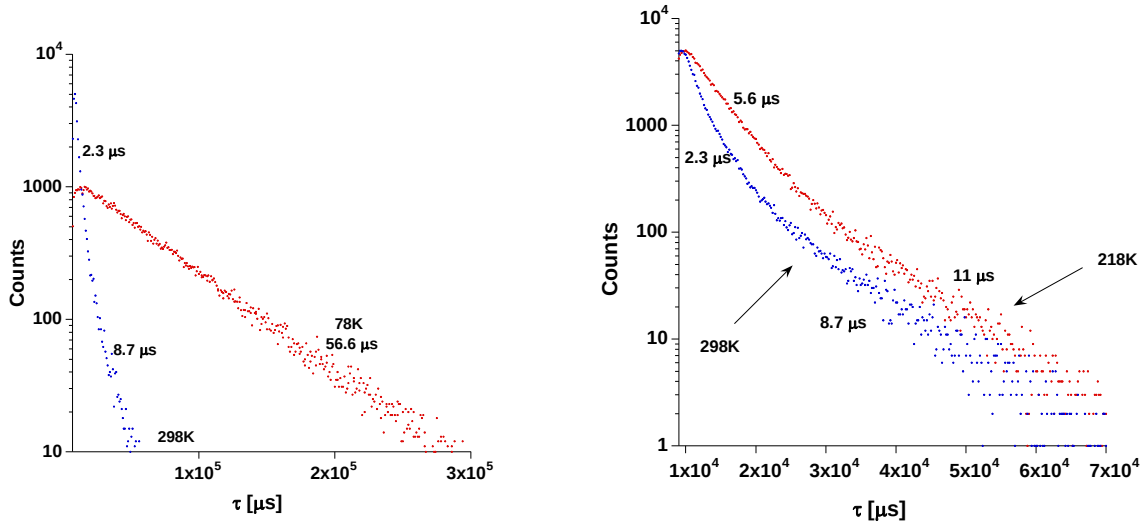

Figure S9: decay profiles at 78K, 218K and 298K for **Cu-1**

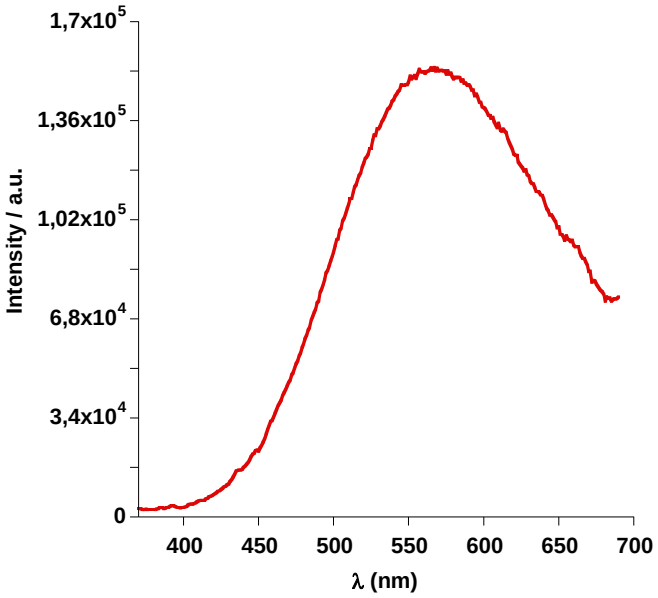

Figure S10: Emission at 298K λ_{max}= 567 nm of **Cu-2** (Ex at 350 nm)

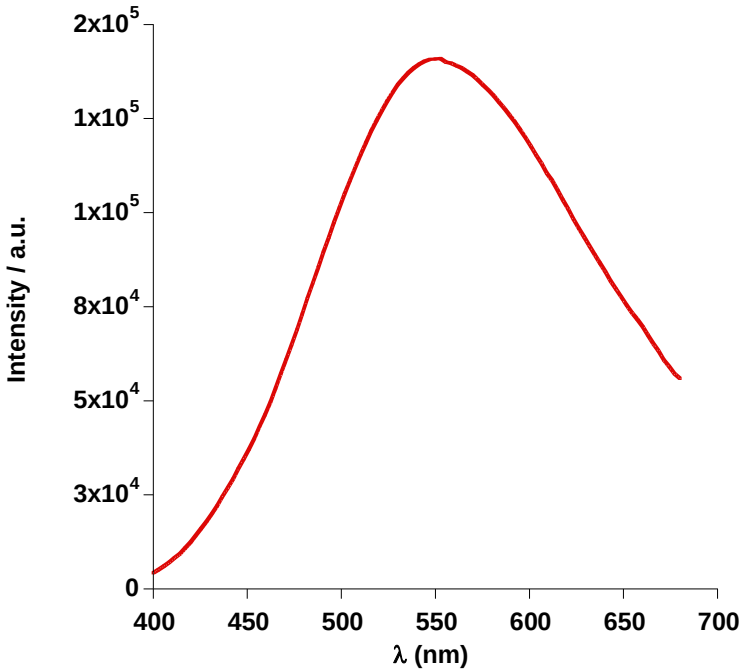

Figure S11: Emission at 298K λ_{max}= 550 nm of **Cu-3** (Ex at 350 nm)

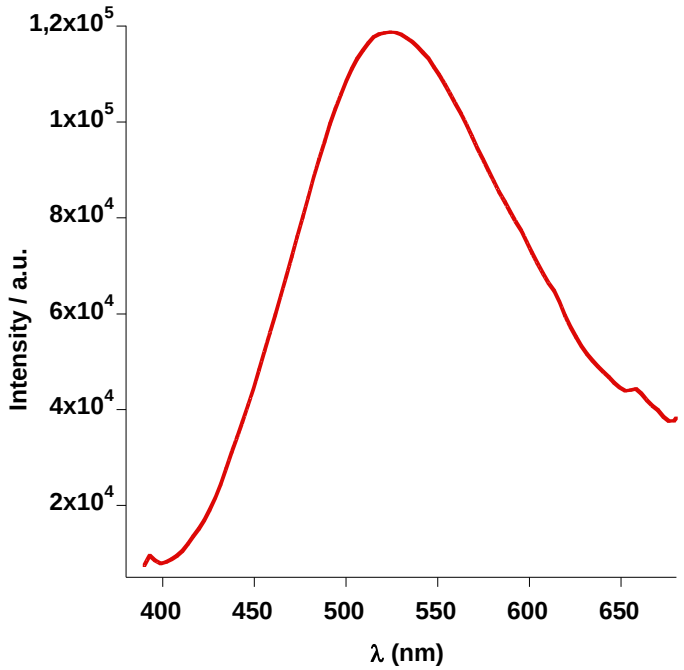

Figure S12: Emission at 298K λ_{max}= 522 nm of **Cu-4** (Ex at 350 nm)

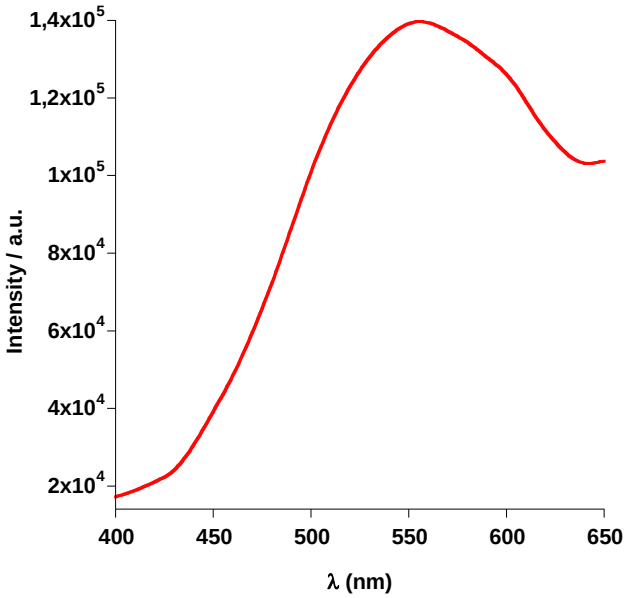

Figure S13: Emission at 298K λ_{max}= 555 nm of **Cu-5** (Ex at 350 nm)

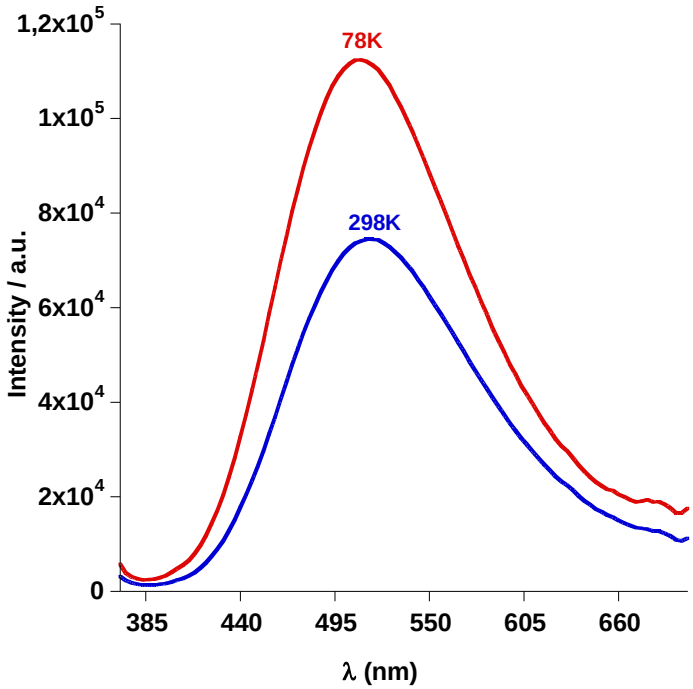

Figure S14: Emissions at 78K λ_{max}= 508 nm and 298K λ_{max}= 515 nm of **Cu-6** (Ex at 360 nm)

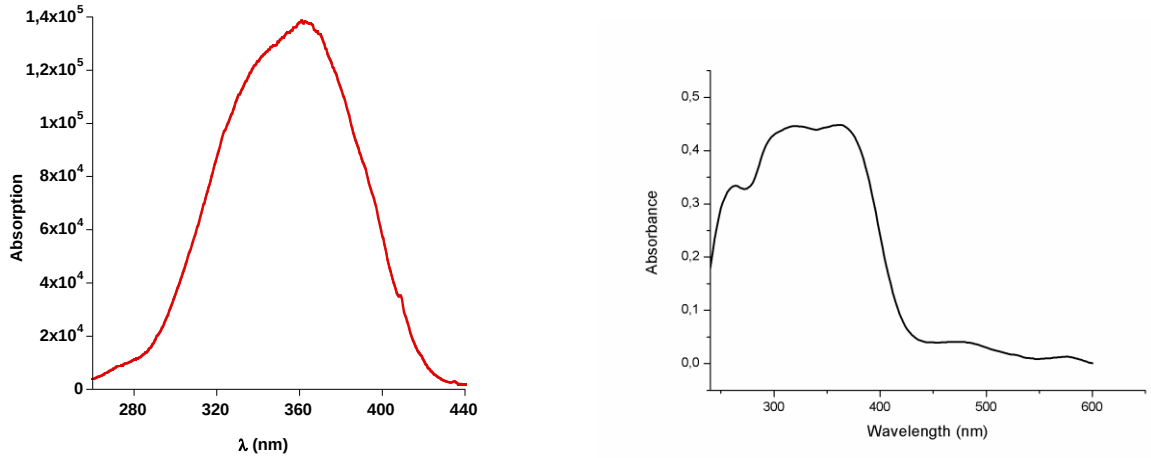

Figure S15: Excitation scan and solid abs spectra of **Cu-6** (298K, λ_{max}= 361 nm)

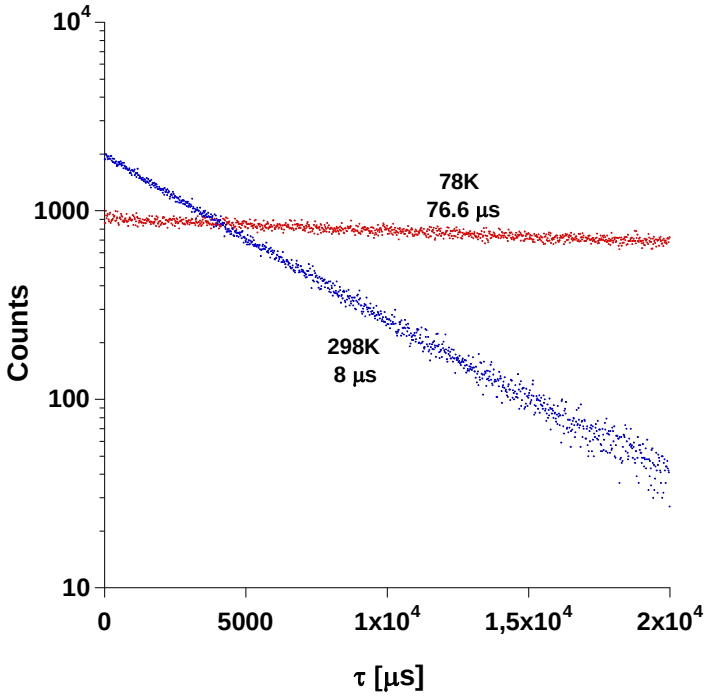

Figure S16: decay profiles at 78K and 298K for **Cu-6**

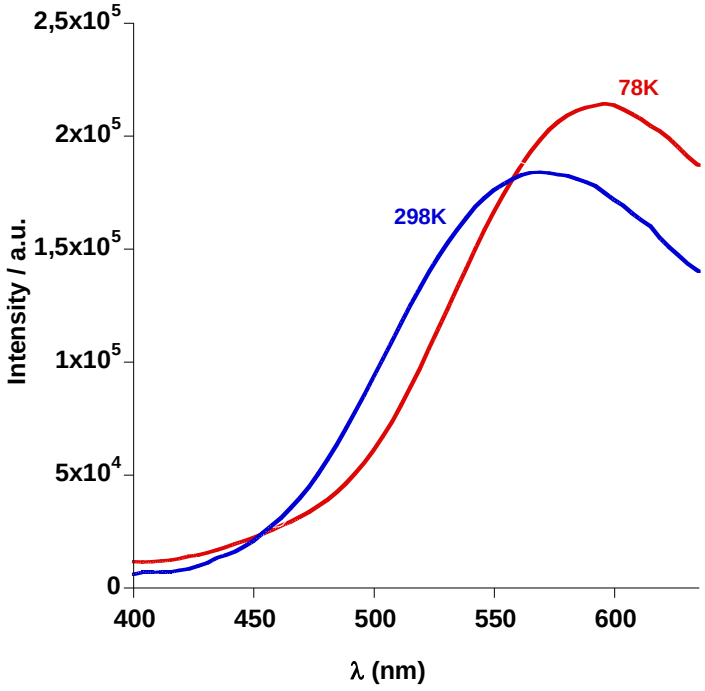

Figure S17: Emissions at 78K λ_{max}= 593 nm and 298K λ_{max}= 568 nm of **Cu-7** (Ex at 340 nm)

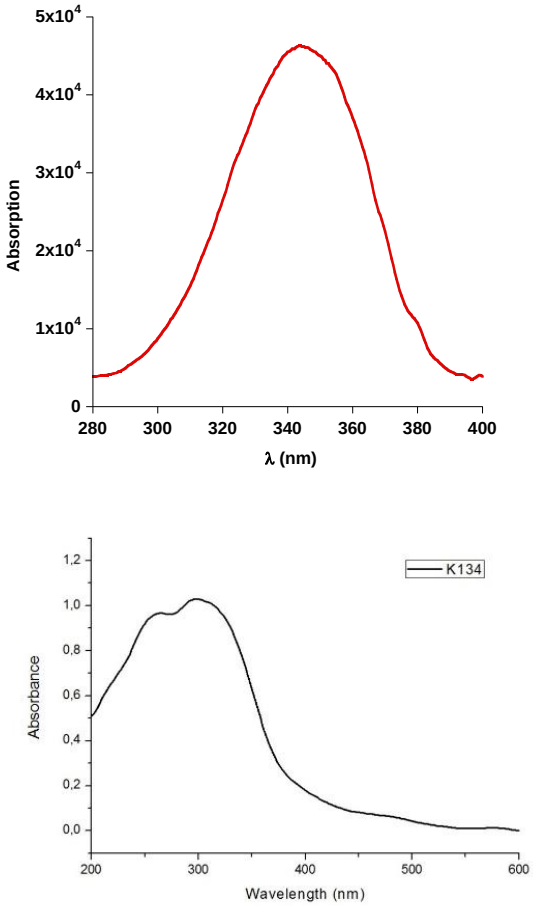

Figure S18: Excitation scan of and solid abs spectra **Cu-7** (298K, λ_{max}= 344 nm)

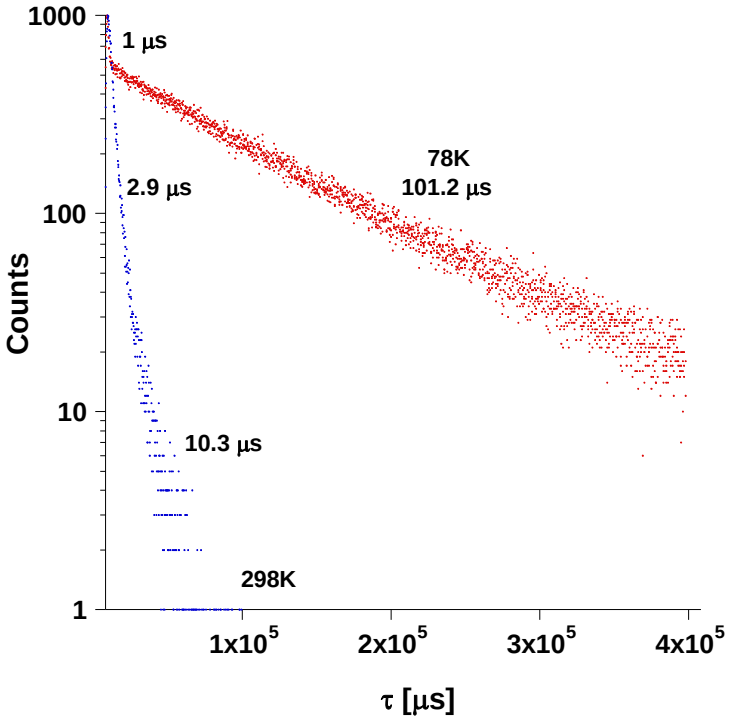

Figure S19: decay profiles at 78K and 298K for **Cu-7**

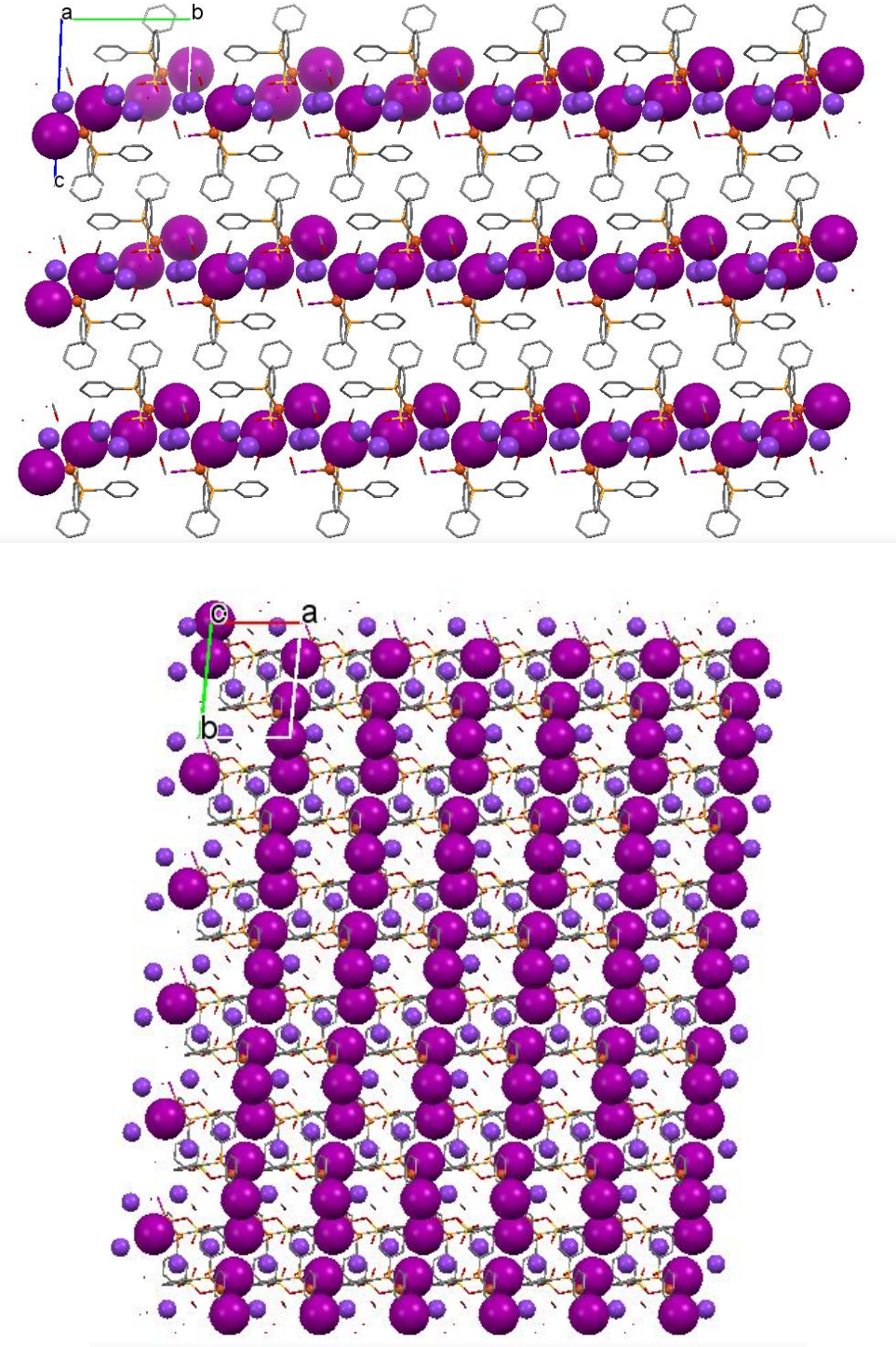

Figure S20: Packing structure for **Cu-6**

Theoretical Part on Cu-1 taking into account solvent effects.

Geometry:

Optimized geometrical parameters of the binuclear complex obtained for the ground state S0 in the gas phase and in solution (in CH_3OH) as well as the X-ray ones are given in Table S1.

As it can be seen in Table S1, the S0 optimized geometry departs slightly from the symmetry of the X-ray structure. We remind that no symmetry constraint has been applied during the geometry optimization process of the complex. The agreement between the X-ray and computed structures is correct, the mean deviation between the computed bond lengths and the X-ray one being less than 5%. We checked that these small deviations can be reduced when using a more extended basis set. Not surprisingly, small deviations are observed between optimized dihedral angles and X-ray ones, packing effects being at work in the crystal, whereas deviations between bond angles is higher than expected, especially in the case of P-Cu-O angle, namely 117.3° and 114.7° for computed values *vs.* 133.4° for the X-ray ones.

Table S1: X-ray and computed geometrical parameters of the ground state.

Atoms (numbers)	S_0 Calc. gaz	X-ray	S_0 Calc. solvent
Cu-P (88-86)	2.244	2.153	2.255
Cu-P (44-42)	2.260	2.153	2.260
Cu-O (44-77)	2.061	2.099	2.065
Cu-O(88-33)	2.029	2.099	2.080
Cu-O (44-40)	2.271	2.190	2.317
Cu-O (88-84)	2.293	2.190	2.232
Cu-O(OHCH3) (44-34)	2.176	2.040	2.163
Cu-O(OHCH3) (88-78)	2.263	2.040	2.189
Cu-O-S (bridge:44-77-87)	119.76	121.96	124.42
Cu-O-S (bridge:88-84-87)	107.62	113.49	110.16
Cu-O-S (bridge:88-33-43)	121.67	121.96	124.21
Cu-O-S (bridge:44-40-43)	111.78	113.49	109.74

P-Cu-O (42-44-34)	117.33	133.43	119.83
P-Cu-O (bridge:42-44-40)	96.53	100.48	96.23
Cu-O-S-O (44-77-87-84)	-55.74	-52.97	-61.33
Cu-O-S-O (44-40-43-33)	36.36	46.15	35.29
P-Cu-O-S (42-44-77-87)	13.37	6.51	14.05
Cu-O-P-O (88-33-43-40)	48.03	52.97	60.64
Cu-O-P-O (88-84-87-77)	-32.17	-46.15	-34.90

The optimized structure has been shown to be thermodynamically stable thanks to the computations of the frequencies of its normal modes of vibration which were all real. Based on these satisfying results, it is now possible to discuss the ground state electronic structure of the complex (see manuscript).

Luminescence:

The luminescence wavelength has been deduced from the energy difference between the excited states and the ground state at the CAM-B3LYP level, considering the molecule in the gas phase. The energy of the relaxed triplet state has been estimated doing an unrestricted calculation. The emitting state is the first triplet ^{3}MLCT state. The computed value is equal to 372 nm reminding that absorption is computed at 273 nm in the gas phase.

The complex emits only in the solid state, at *ca*. 515 nm whereas its maximum absorption is at 364 nm. The energy Stokes shift between absorption and emission is equal to 0.93 eV. Moreover, it must be reminded that a strong batochromic shift of the UV-visible absorption band is observed when comparing the spectra of the complex in solution and in the solid state, *i.e.* 270 *vs.* 364 nm. Thus, it is hard to compare optical properties observed for a complex in the solid state phase to those of a single complex in the gas phase or in solution. Anyway we compute an energy Stokes shift *i.e.* 1.20 eV for the complex which of the same order of magnitude as the observed one in the solid state.

Electrochemistry:

The frontier occupied MOs of the considered binuclear complex, *i.e.* HOMO and HOMO-1 exhibit a metallic character (*vide supra*). Moreover, the computed HOMO of the cation, after the geometry optimization, is also metallic. These results indicate that the first and the second oxidation processes are mainly localized on the metallic centres. In the case of the second ionization, this is fully confirmed by the spin density of the cation shown in Figure 3. In this Figure, one can see that the spin density is clearly centred on one copper atom, so that it is this one which will undergo ionization. It is worth noting that the cationic binuclear structure is thermodynamically stable in solution, as checked thanks to the computation of its normal modes of vibration. Furthermore, the computed adiabatic Gibbs first ionization energy, computed as the difference between the Gibbs energies of the neutral and cationic

species, is equal to 5.44 eV, all species being optimized in solution. Under the same conditions, the second adiabatic ionisation energy is computed to be equal to 6.72 eV.

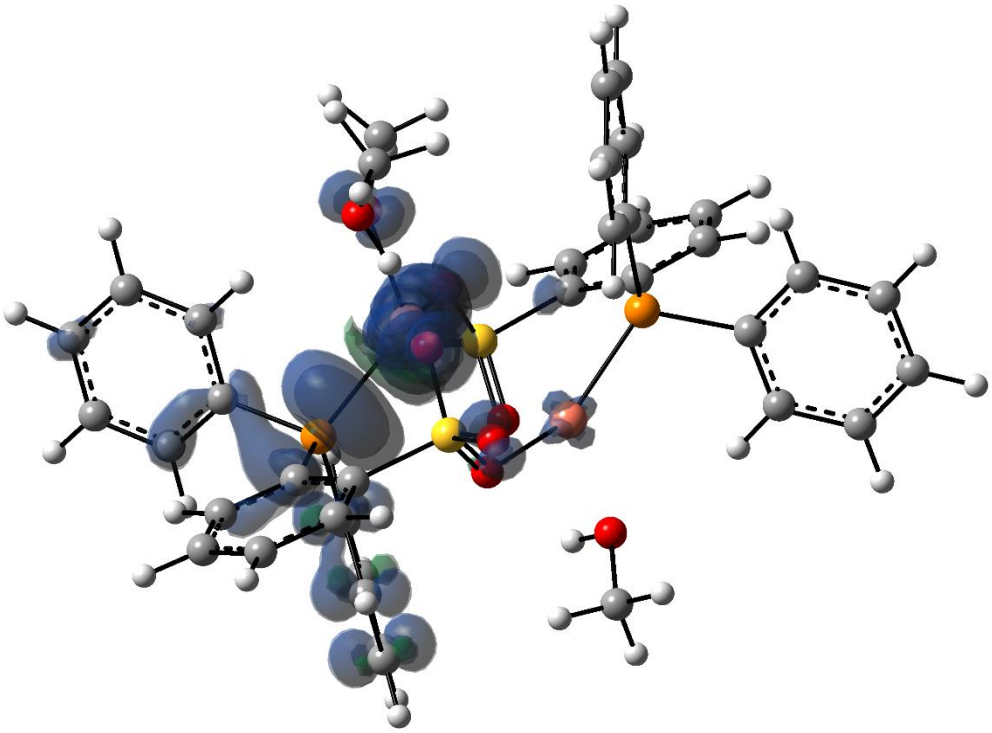

Figure S21: Spin density plot of the cation, isovalue= 0.0009 au

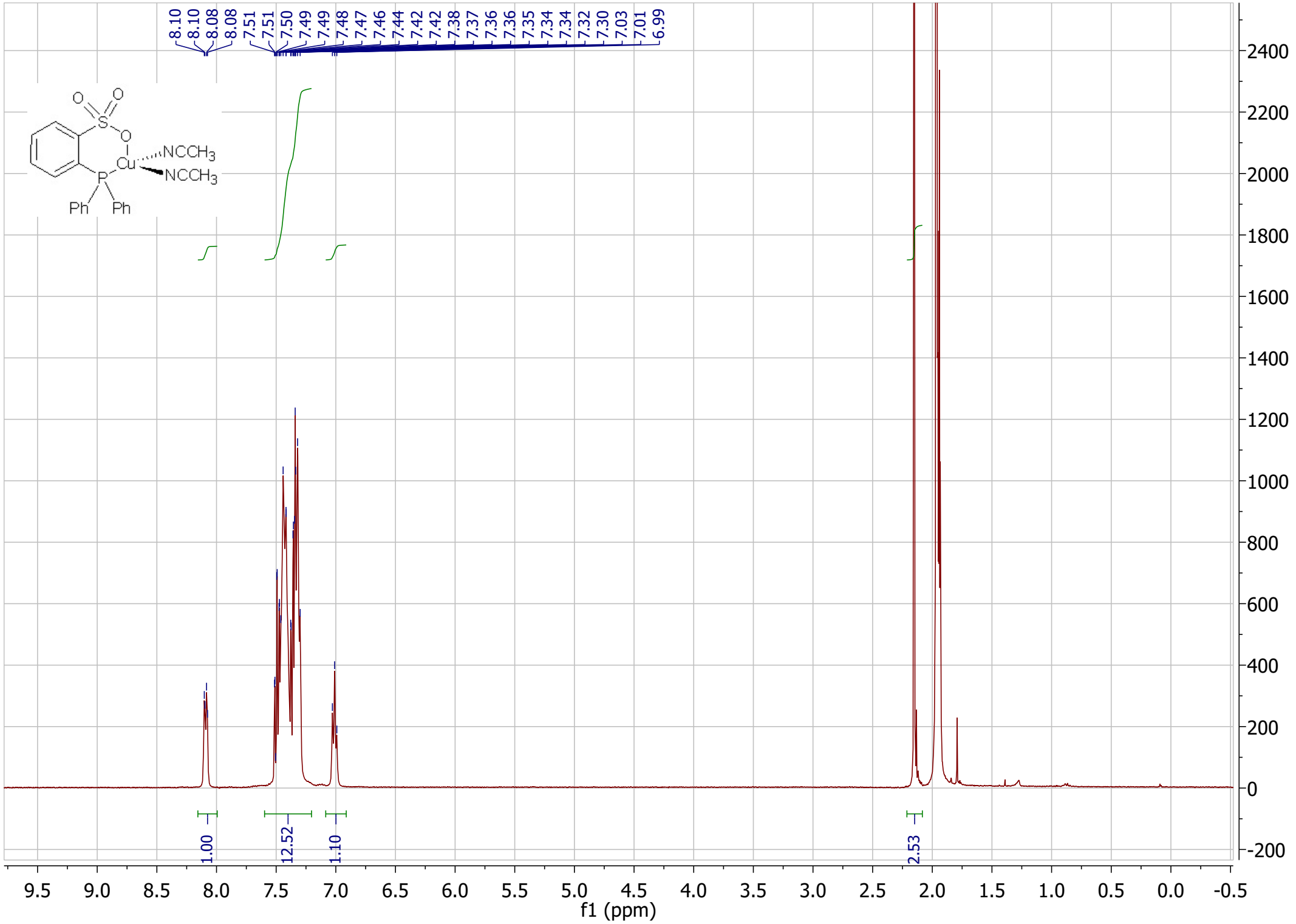
8.10
8.10
8.08
8.08
7.51
7.51
7.50
7.49
7.49
7.48
7.47
7.46
7.44
7.42
7.42
7.38
7.37
7.36
7.36
7.35
7.34
7.34
7.32
7.30
7.03
7.01
6.99
NCCH3
NCCH3
Cu
P
Ph
Ph
1.00
12.52
1.10
2.53
f1 (ppm)

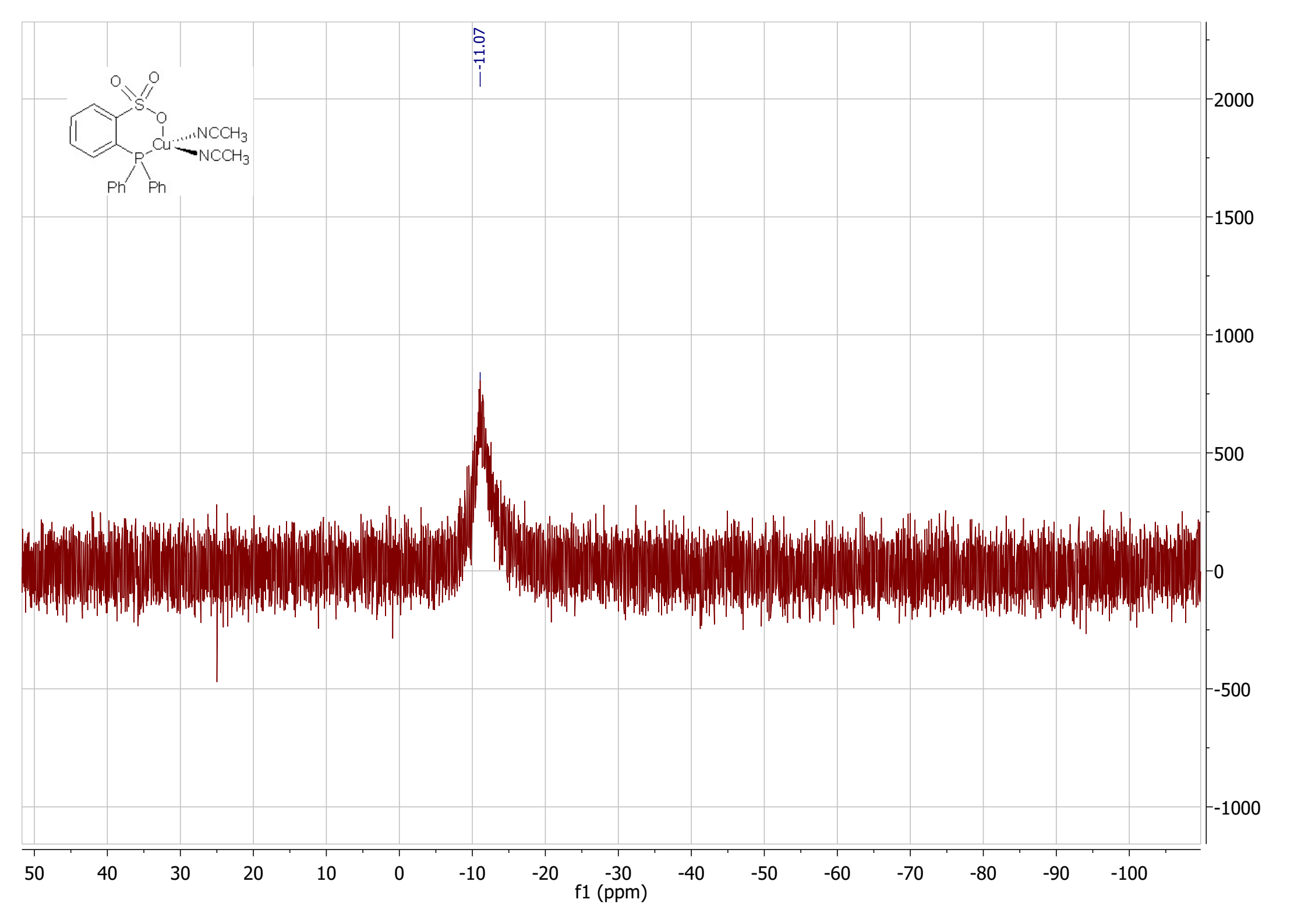
-11.07
2000
1500
1000
500
0
-500
-1000
50
40
30
20
10
0
-10
-20
-30
-40
-50
-60
-70
-80
-90
-100
f1 (ppm)
O
O
S
O
Cu
NCCH3
NCCH3
P
Ph
Ph

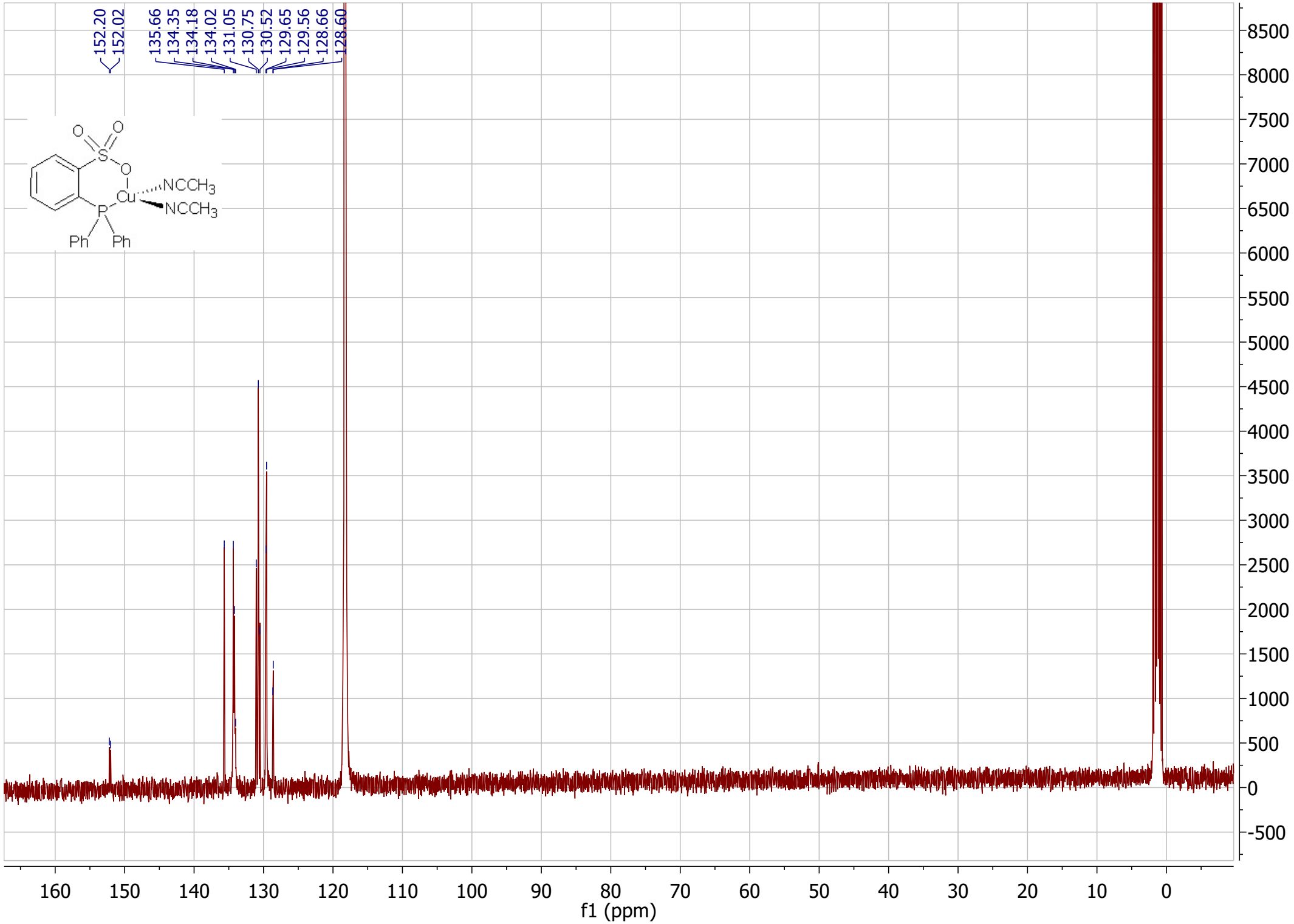
152.20
152.02
135.66
134.35
134.18
134.02
131.05
130.75
130.52
129.65
129.56
128.66
128.60
O
O
S
O
Cu
NCCH3
NCCH3
P
Ph
Ph
8500
8000
7500
7000
6500
6000
5500
5000
4500
4000
3500
3000
2500
2000
1500
1000
500
0
-500
160
150
140
130
120
110
100
90
80
70
60
50
40
30
20
10
0
f1 (ppm)

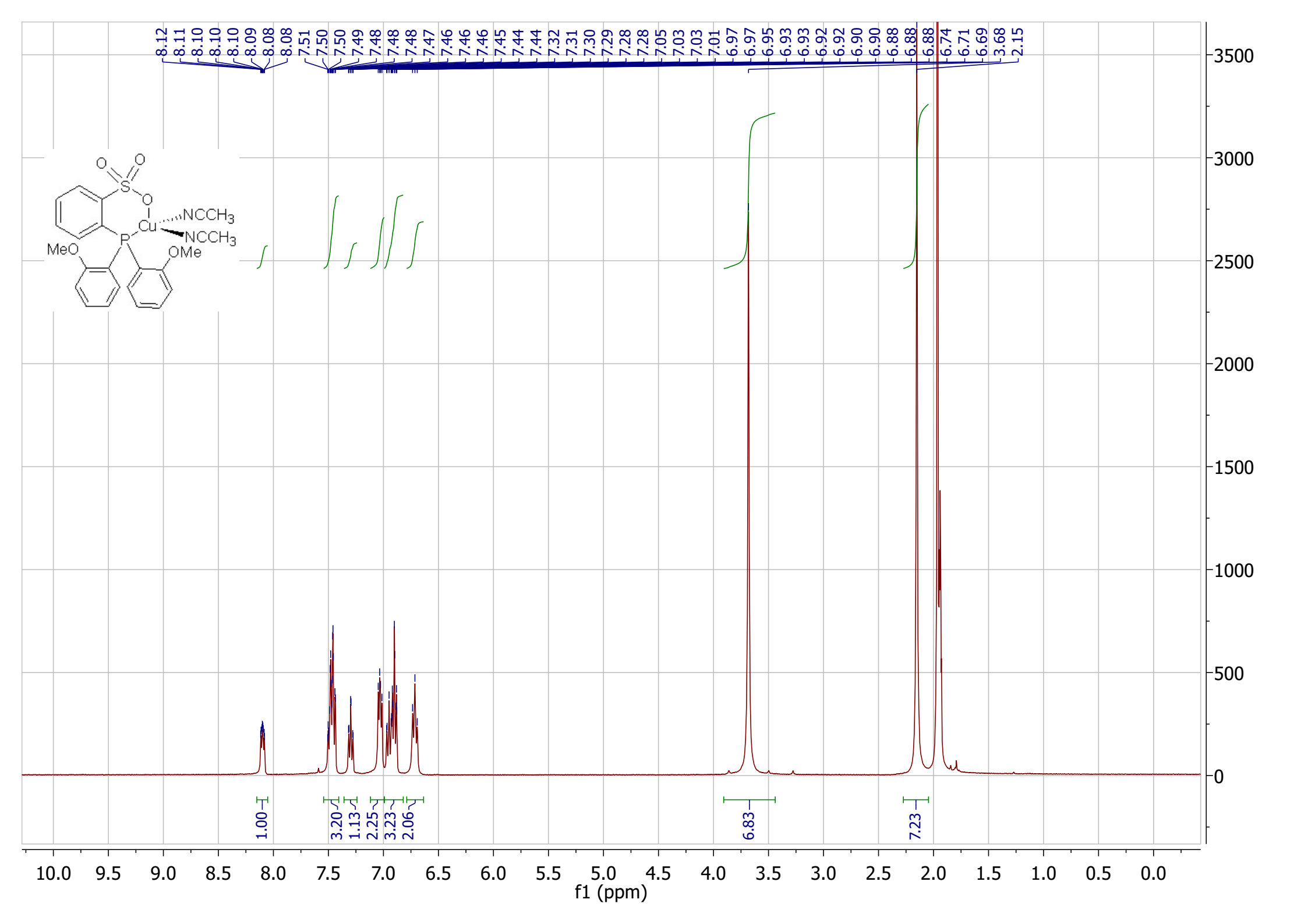
8.12 8.11 8.10 8.10 8.10 8.09 8.08 8.08 7.51 7.50 7.50 7.49 7.48 7.48 7.48 7.47 7.46 7.46 7.46 7.45 7.44 7.44 7.32 7.31 7.30 7.29 7.28 7.28 7.05 7.03 7.03 7.01 6.97 6.97 6.95 6.93 6.93 6.92 6.92 6.90 6.90 6.88 6.88 6.88 6.74 6.71 6.69 3.68 2.15
O
O
S
O
Cu
NCCH3
NCCH3
P
MeO
OMe
3500
3000
2500
2000
1500
1000
500
0
1.00
3.20
1.13
2.25
3.23
2.06
6.83
7.23
10.0 9.5 9.0 8.5 8.0 7.5 7.0 6.5 6.0 5.5 5.0 4.5 4.0 3.5 3.0 2.5 2.0 1.5 1.0 0.5 0.0
f1 (ppm)

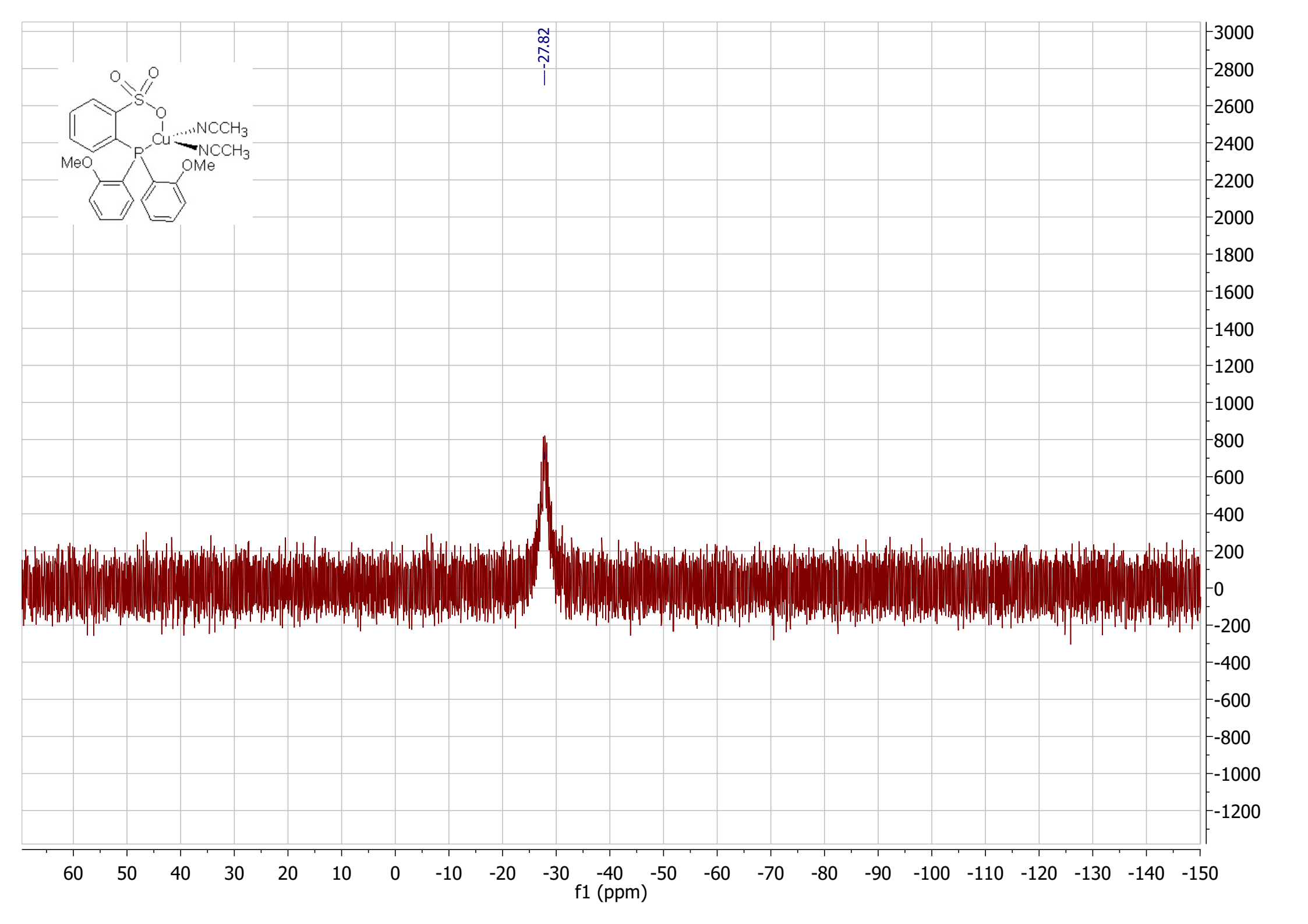
-27.82
3000
2800
2600
2400
2200
2000
1800
1600
1400
1200
1000
800
600
400
200
0
-200
-400
-600
-800
-1000
-1200
60
50
40
30
20
10
0
-10
-20
-30
-40
-50
-60
-70
-80
-90
-100
-110
-120
-130
-140
-150
f1 (ppm)
O
O
S
O
Cu
NCCH3
NCCH3
P
MeO
OMe

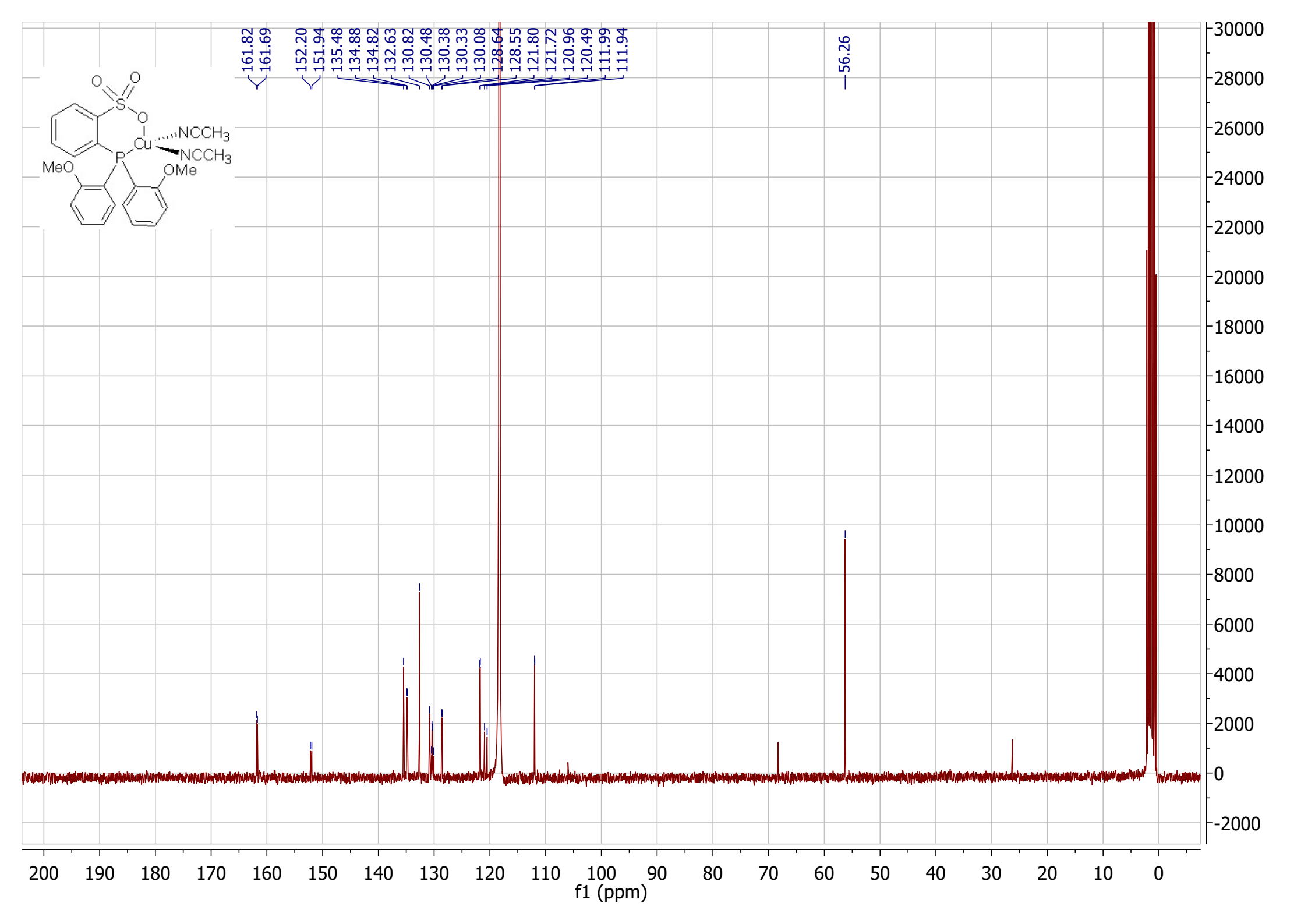
161.82
161.69
152.20
151.94
135.48
134.88
134.82
132.63
130.82
130.48
130.38
130.33
130.08
128.64
128.55
121.80
121.72
120.96
120.49
111.99
111.94
56.26
O
O
S
O
Cu
NCCH3
NCCH3
P
MeO
OMe
30000
28000
26000
24000
22000
20000
18000
16000
14000
12000
10000
8000
6000
4000
2000
0
-2000
200
190
180
170
160
150
140
130
120
110
100
90
80
70
60
50
40
30
20
10
0
f1 (ppm)

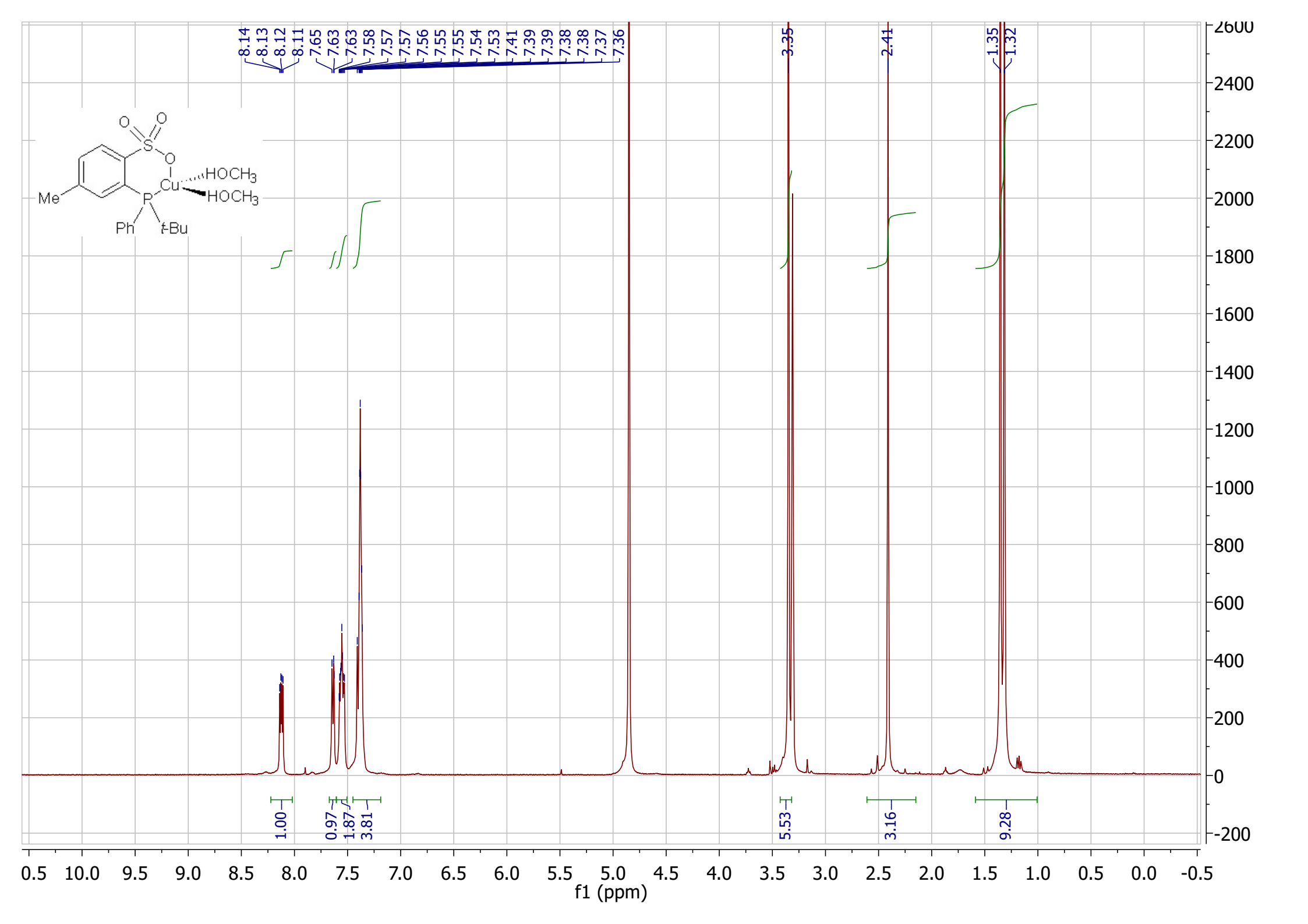
8.14
8.13
8.12
8.11
7.65
7.63
7.63
7.58
7.57
7.57
7.56
7.55
7.55
7.54
7.53
7.41
7.39
7.39
7.38
7.38
7.37
7.36
3.35
2.41
1.35
1.32
Me
Ph
t-Bu
Cu
HOCH3
HOCH3
1.00
0.97
1.87
3.81
5.53
3.16
9.28
f1 (ppm)

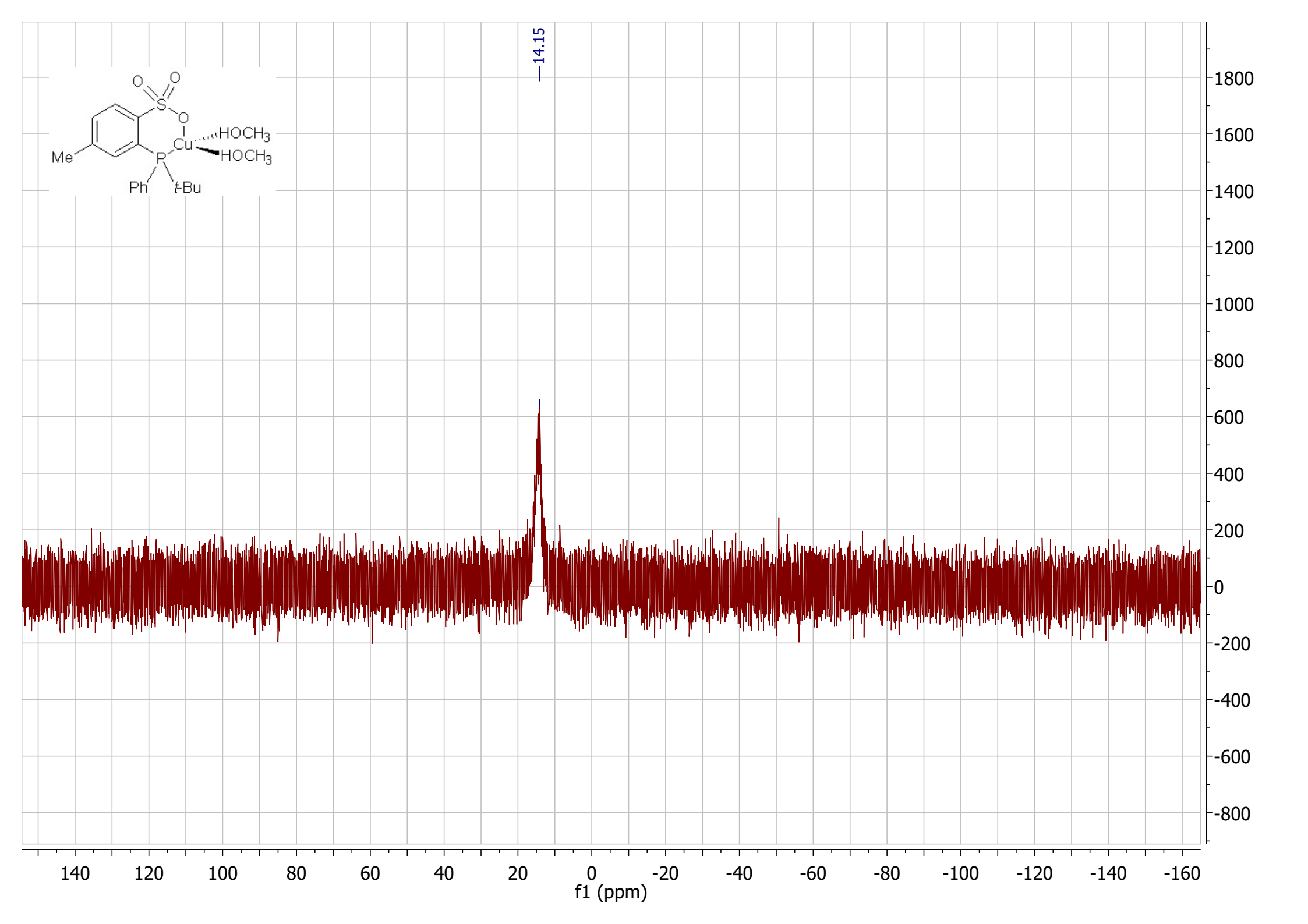
14.15
1800
1600
1400
1200
1000
800
600
400
200
0
-200
-400
-600
-800
140
120
100
80
60
40
20
0
-20
-40
-60
-80
-100
-120
-140
-160
f1 (ppm)
O
O
S
O
Cu
HOCH3
HOCH3
Me
P
Ph
t-Bu

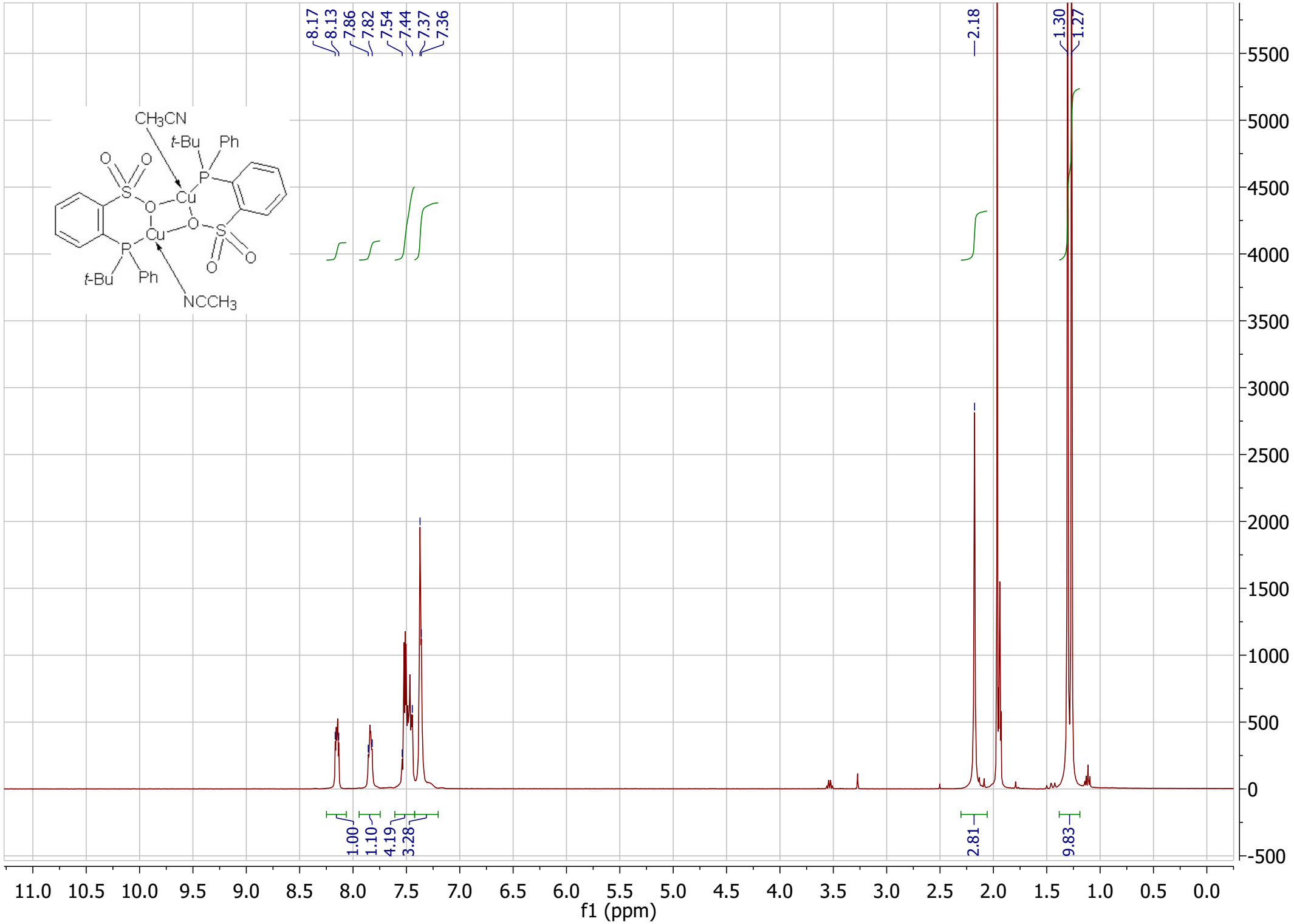
8.17
8.13
7.86
7.82
7.54
7.44
7.37
7.36
2.18
1.30
1.27
CH3CN
t-Bu
Ph
P
Cu
O
S
t-Bu
Ph
NCCH3
1.00
1.10
4.19
3.28
2.81
9.83
5500
5000
4500
4000
3500
3000
2500
2000
1500
1000
500
0
-500
11.0
10.5
10.0
9.5
9.0
8.5
8.0
7.5
7.0
6.5
6.0
5.5
5.0
4.5
4.0
3.5
3.0
2.5
2.0
1.5
1.0
0.5
0.0
f1 (ppm)

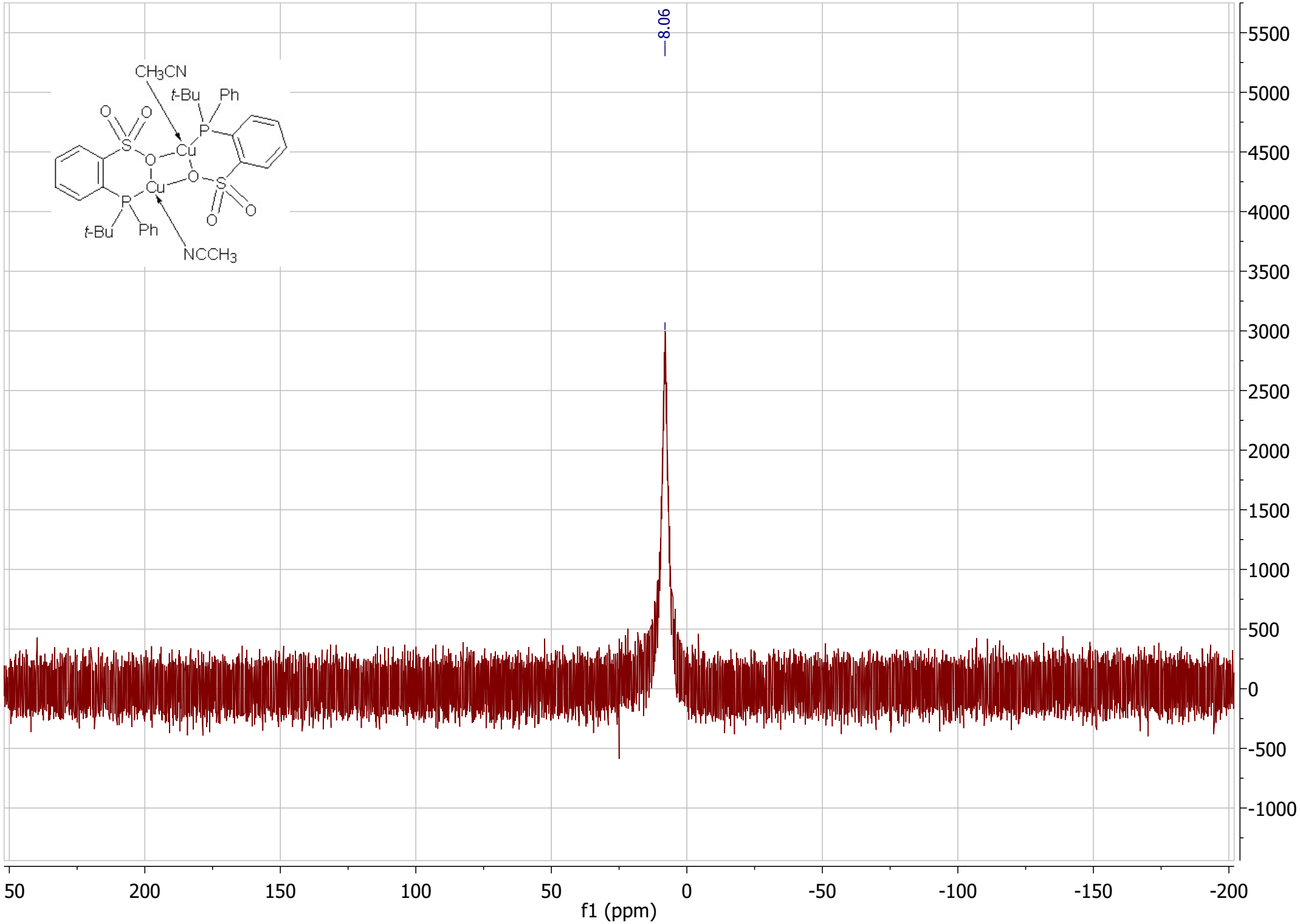
8.06
CH3CN
t-Bu
Ph
O
O
S
O
Cu
P
Cu
O
S
O
O
P
t-Bu
Ph
NCCH3
5500
5000
4500
4000
3500
3000
2500
2000
1500
1000
500
0
-500
-1000
50
200
150
100
50
0
-50
-100
-150
-200
f1 (ppm)

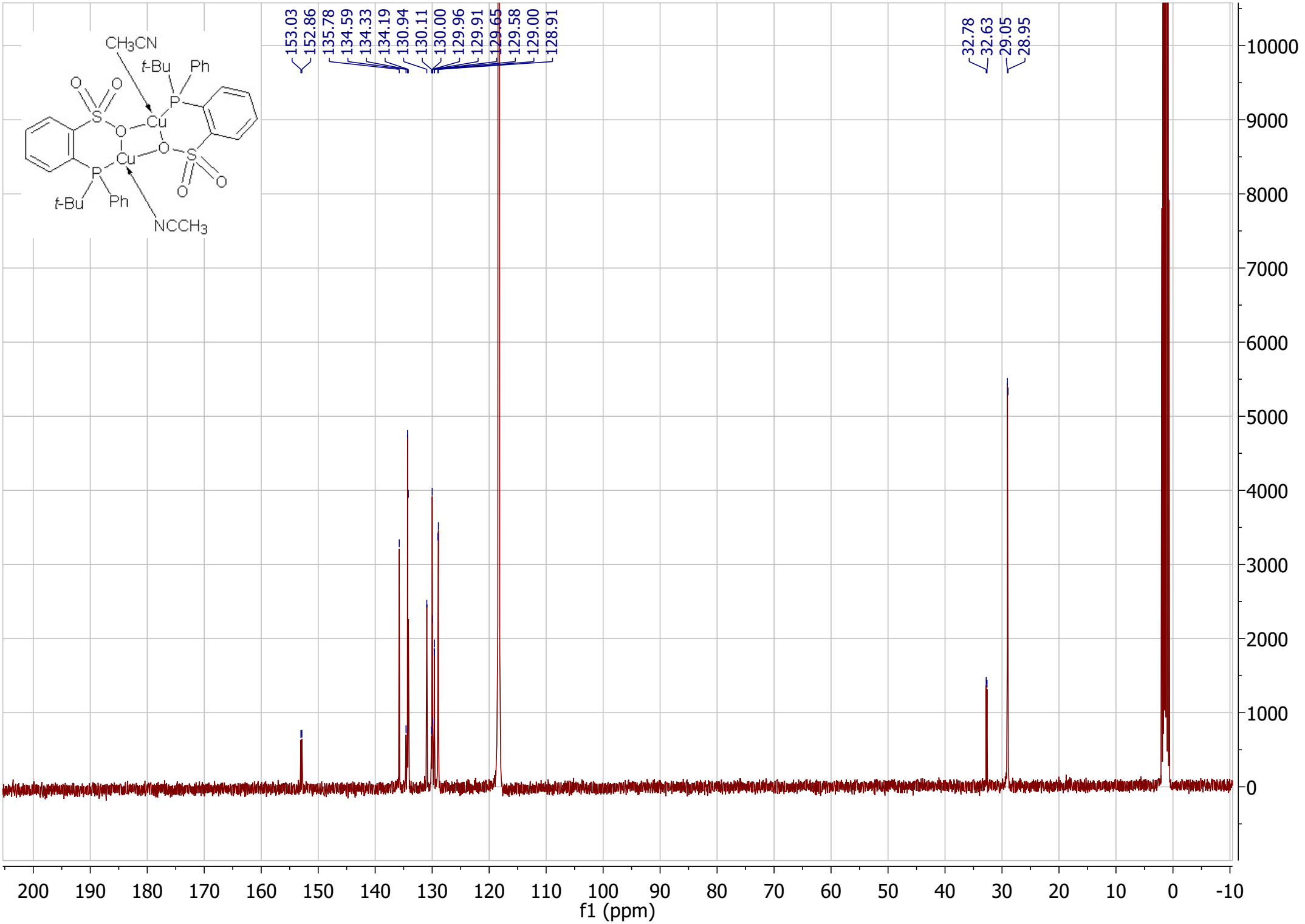
153.03
152.86
135.78
134.59
134.33
134.19
130.94
130.11
130.00
129.96
129.91
129.65
129.58
129.00
128.91
32.78
32.63
29.05
28.95
CH3CN
t-Bu
Ph
NCCH3
10000
9000
8000
7000
6000
5000
4000
3000
2000
1000
0
200
190
180
170
160
150
140
130
120
110
100
90
80
70
60
50
40
30
20
10
0
-10
f1 (ppm)

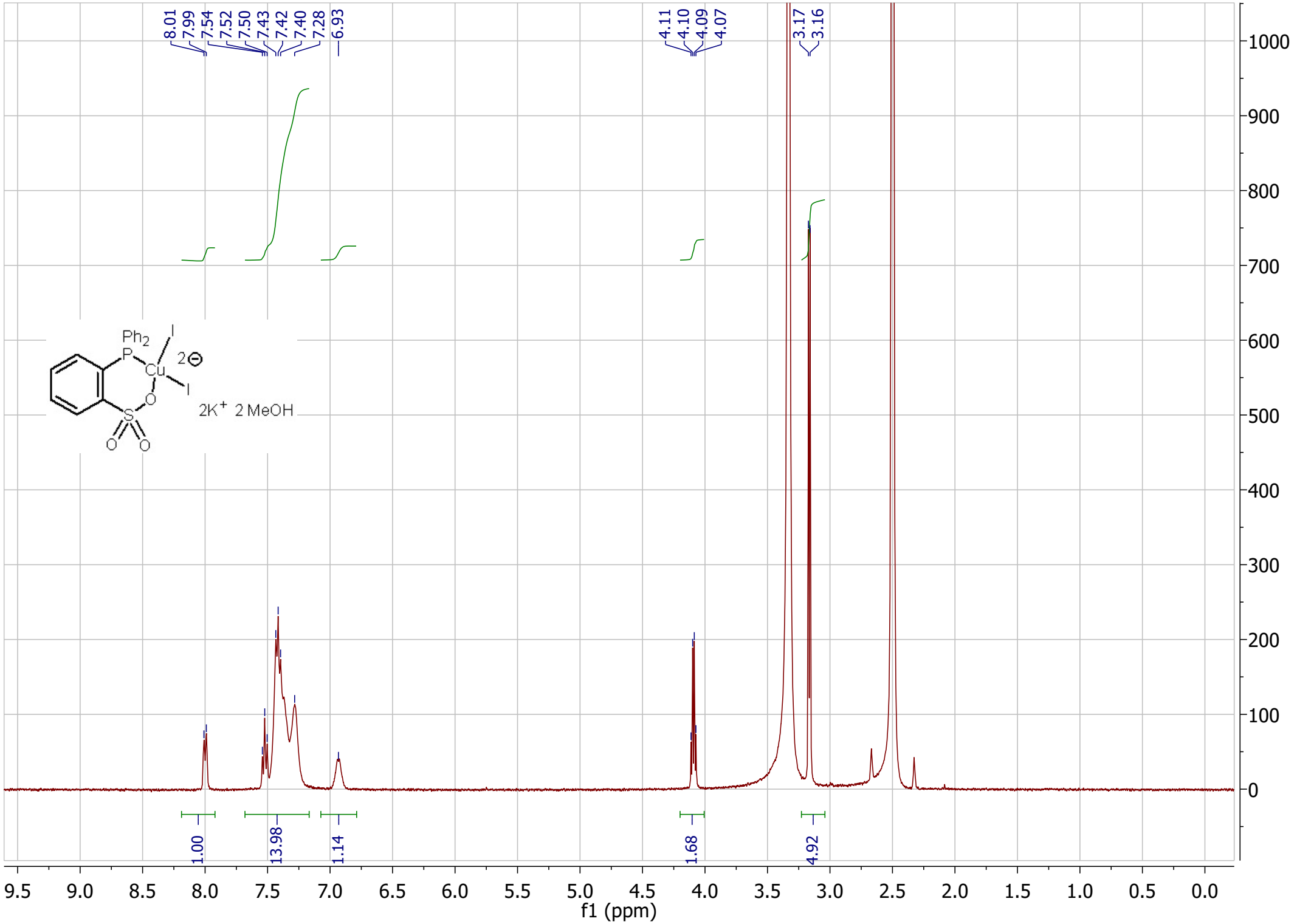
8.01
7.99
7.54
7.52
7.50
7.43
7.42
7.40
7.28
6.93
4.11
4.10
4.09
4.07
3.17
3.16
Ph2
P
Cu
I
I
2⊖
O
S
O
O
2K+ 2 MeOH
1.00
13.98
1.14
1.68
4.92
1000
900
800
700
600
500
400
300
200
100
0
9.5
9.0
8.5
8.0
7.5
7.0
6.5
6.0
5.5
5.0
4.5
4.0
3.5
3.0
2.5
2.0
1.5
1.0
0.5
0.0
f1 (ppm)

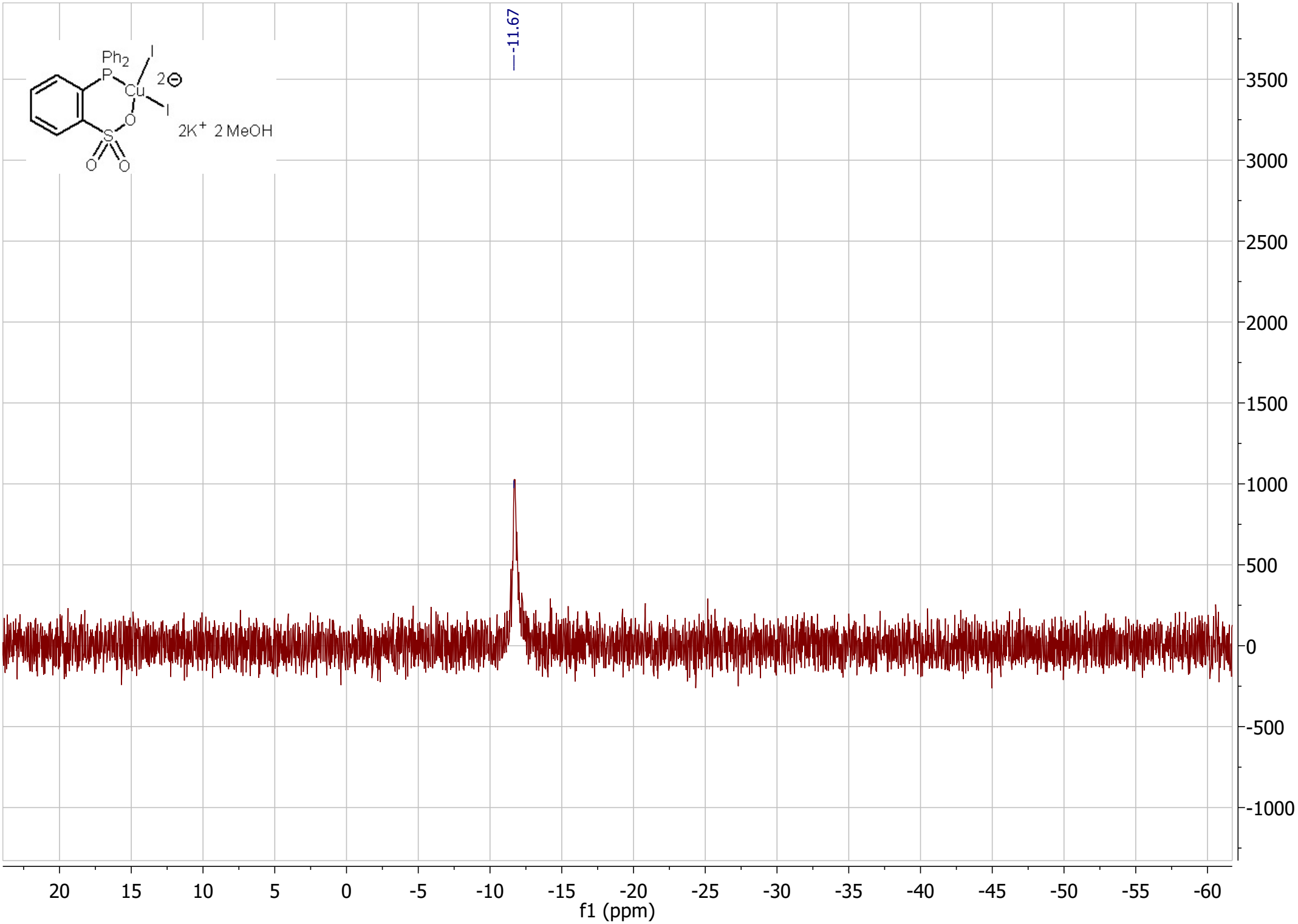
-11.67
Ph2
P
Cu
I
I
2⊖
O
S
O
O
2K+ 2 MeOH
3500
3000
2500
2000
1500
1000
500
0
-500
-1000
20
15
10
5
0
-5
-10
-15
-20
-25
-30
-35
-40
-45
-50
-55
-60
f1 (ppm)

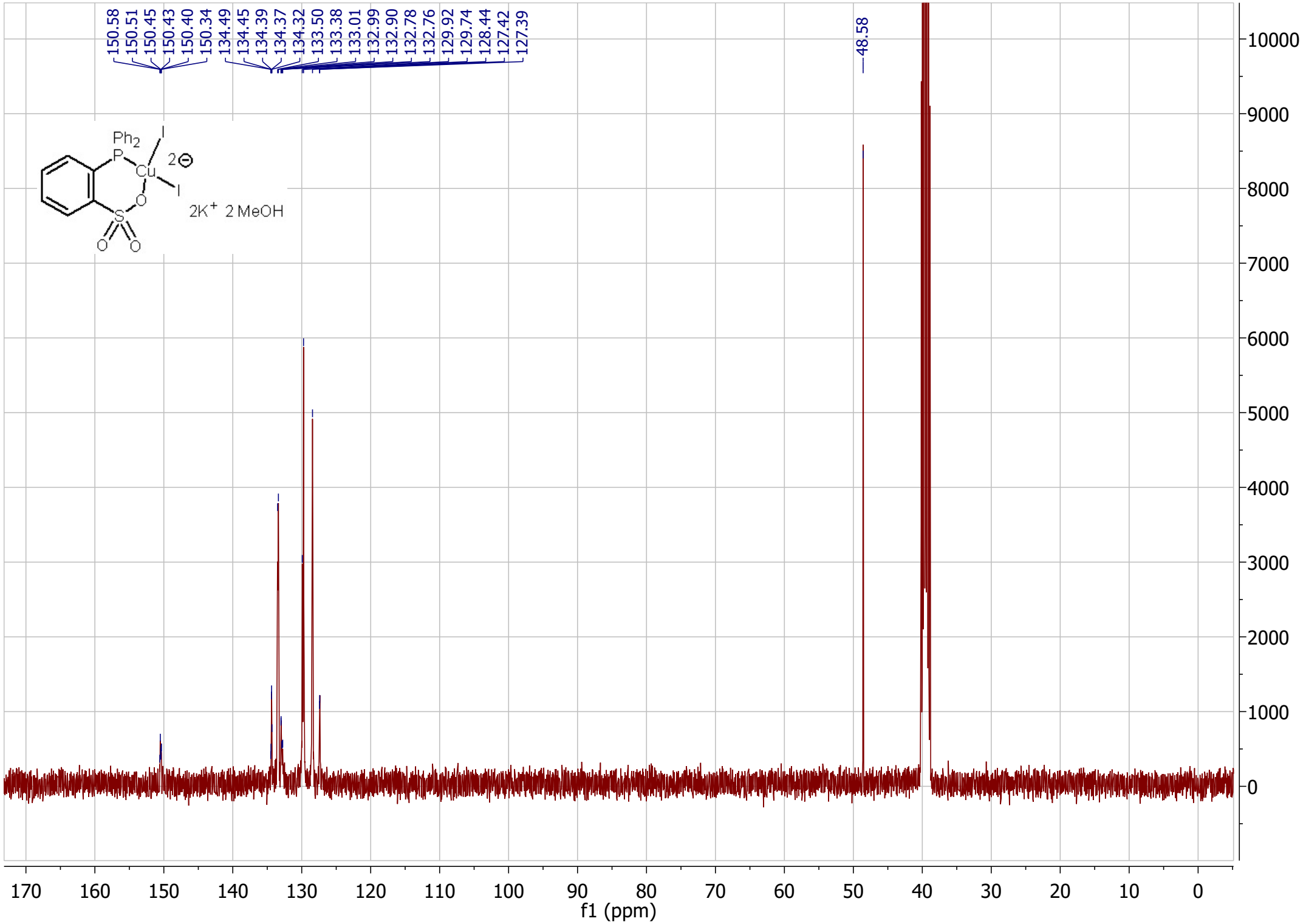
150.58
150.51
150.45
150.43
150.40
150.34
134.49
134.45
134.39
134.37
134.32
133.50
133.38
133.01
132.99
132.90
132.78
132.76
129.92
129.74
128.44
127.42
127.39
48.58
Ph2
P
Cu
I
I
2⊖
O
S
O
O
2K+ 2 MeOH
10000
9000
8000
7000
6000
5000
4000
3000
2000
1000
0
170
160
150
140
130
120
110
100
90
80
70
60
50
40
30
20
10
0
f1 (ppm)

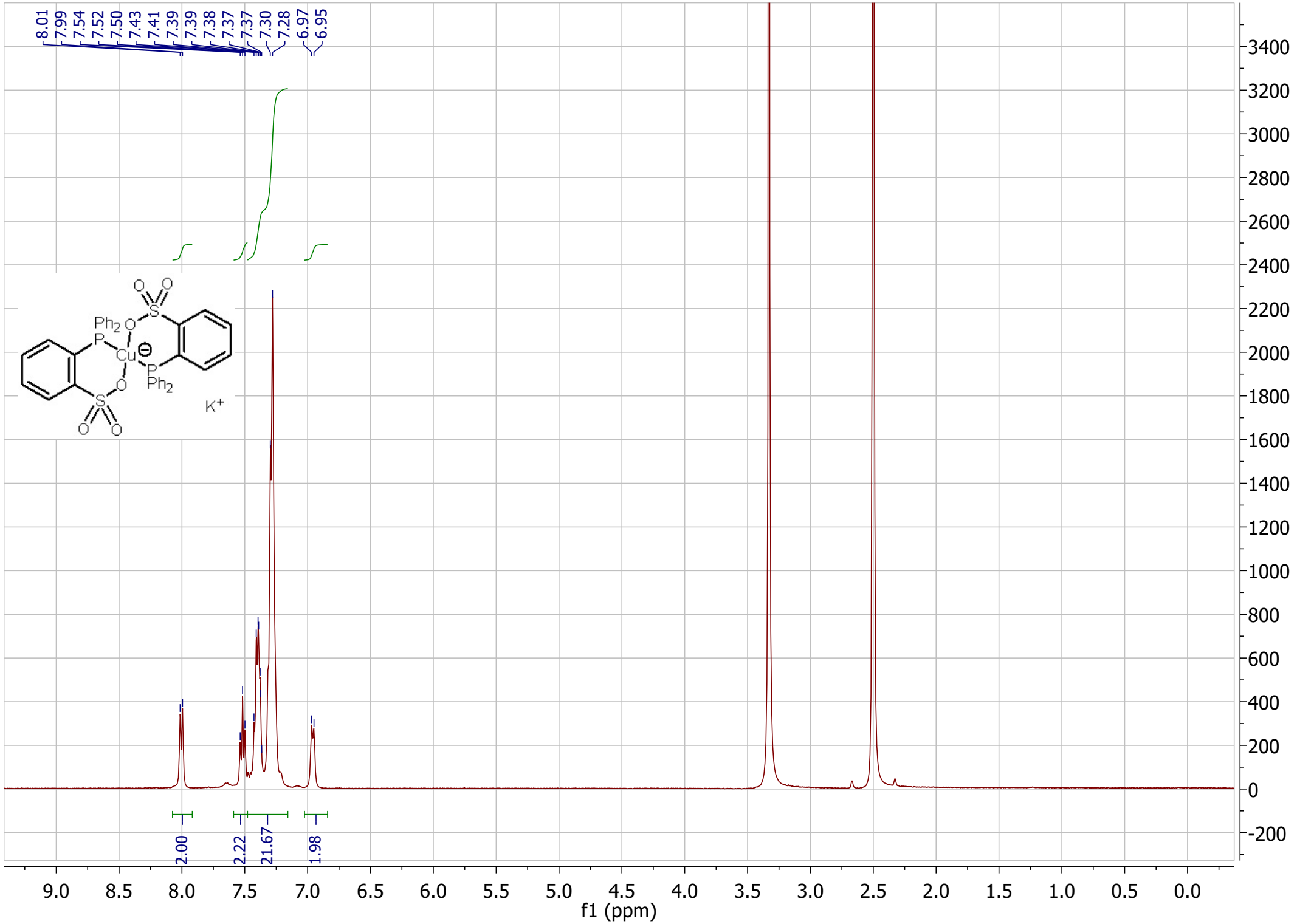
8.01
7.99
7.54
7.52
7.50
7.43
7.41
7.39
7.39
7.38
7.37
7.37
7.30
7.28
6.97
6.95
Ph2
P
O
Cu
O
P
Ph2
S
O
O
O
O
S
O
K+
2.00
2.22
21.67
1.98
9.0
8.5
8.0
7.5
7.0
6.5
6.0
5.5
5.0
4.5
4.0
3.5
3.0
2.5
2.0
1.5
1.0
0.5
0.0
f1 (ppm)
3400
3200
3000
2800
2600
2400
2200
2000
1800
1600
1400
1200
1000
800
600
400
200
0
-200

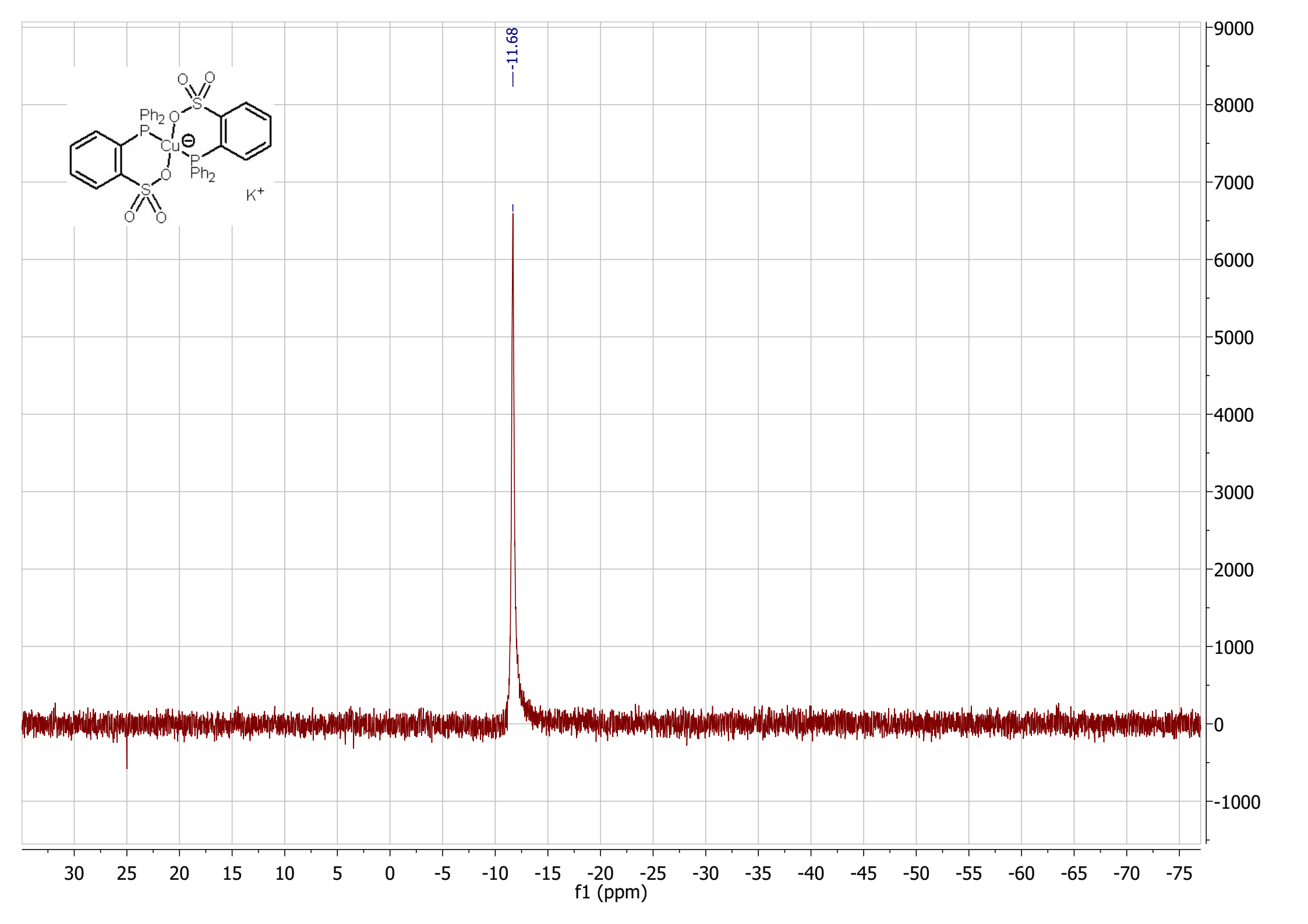
-11.68
9000
8000
7000
6000
5000
4000
3000
2000
1000
0
-1000
30
25
20
15
10
5
0
-5
-10
-15
-20
-25
-30
-35
-40
-45
-50
-55
-60
-65
-70
-75
f1 (ppm)
Ph2
P
O
S
Cu
K+

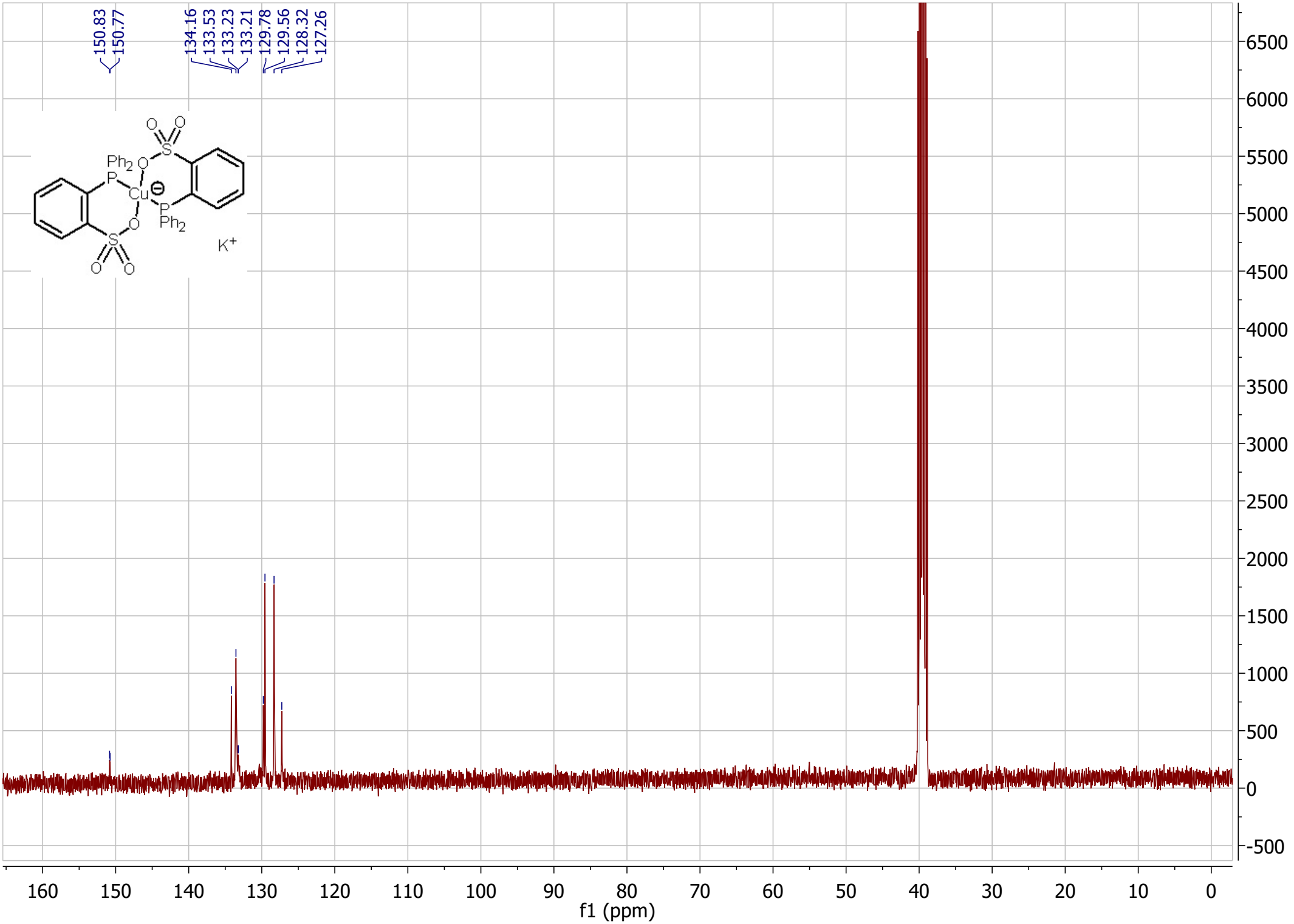
150.83
150.77
134.16
133.53
133.23
133.21
129.78
129.56
128.32
127.26
Ph2
P
O
Cu
P
Ph2
O
S
O
O
S
O
O
K+
6500
6000
5500
5000
4500
4000
3500
3000
2500
2000
1500
1000
500
0
-500
160
150
140
130
120
110
100
90
80
70
60
50
40
30
20
10
0
f1 (ppm)